TI Designs
Low-Power PIR Motion Detector With Sub-1GHz Wireless Connectivity Enabling 10-Year Coin Cell Battery Life

TI Designs

This TI Design uses Texas Instruments' nano-power operational amplifiers, comparators, and the SimpleLink™ ultra-low-power sub-1GHz wireless microcontroller (MCU) platform to demonstrate an ultra-low-power motion detector, leading to extremely long battery life and no required wiring.

Design Resources

TIDA-00489	Design Folder
LPV802	Product Folder
TLV3691	Product Folder
CC1310	Product Folder

TI E2E™ Community — ASK Our E2E Experts

Design Features

- Use of Nano-Power Analog for Ultra-Low-Power Design Resulting in 10-Year Battery Life From Single CR2032 Coin Cell
- Low Standby Current of 1.65 μA (PIR Sensor Remains Active in Standby)
- Ultra-Low Active State Current Due to Low Active Processor and Radio Transmit Currents (1.12 mA for 104.1 ms)
- Interrupt Driven Sub-1GHz Wireless Communication of Motion for Increased Power Savings
- Motion Sensitivity up to 30 ft

Featured Applications

- Building Automation
- Intrusion Detection
- Occupancy Detection
- Motion Detection
- Room Monitors
- Battery Powered Systems

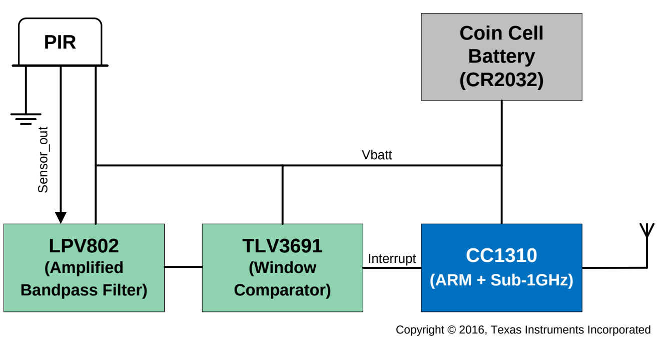

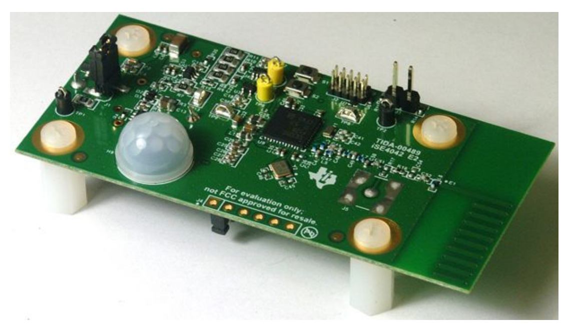

An IMPORTANT NOTICE at the end of this TI reference design addresses authorized use, intellectual property matters and other important disclaimers and information.

1 Key System Specifications

Table 1. Key System Specifications

PARAMETER	SPECIFICATIONS	DETAILS
Input power source	CR2032 Lithium-ion coin cell battery (3.0-V nominal voltage)	Section 2.4
Sensor type	PIR (Pyroelectric or Passive InfraRed)	Section 2.5
Average active-state current consumption	1.12 mA	Section 8.1
Active-state duration	104.1 ms	Section 8.1
Average standby-state current consumption	2.3 µA	Section 8.1
Standby-state duration	1 minute of no motion detected	Section 4.4
Sleep-state current consumption	1.65 µA	Section 8.1
Movements per hour assumed for lifetime calculation	≥10 per hour average over the battery lifetime (worst case)	Section 8.2
Estimated battery life	> 10 years	Section 8.2
Motion sensing range	30 feet nominal	Section 8.3.1
Radio transmission range	> 200 meters	Section 8.3.2
Operating temperature	–30°C to 60°C (limited by CR2032 coin cell operating range)	Section 2.4
Operating humidity	20 to 70%	Section 7.3.1
Vibration		Section 8.3.4
RF immunity	30 V/m from 10 kHz to 1 GHz	Section 8.3.3
Working environment	Indoor and outdoor	Section 2.4
Form factor	35×75-mm rectangular PCB	Section 9.5

2 System Description

Many industrial and building automation systems use motion detectors to control different functions based on human presence, such as lighting, for achieving higher efficiency of those functions by turning them off when not needed. Additionally, these systems require increasing numbers of wireless sensor nodes to reduce the installation costs and the make the systems more flexible for future expansion by eliminating wiring. However, one of the major limitations for a large wireless network is power. Because these systems are battery powered, the maintenance cost associated with periodic battery replacement can become prohibitive. Depending on the power consumption and battery configuration, typical battery-powered PIR motion detectors can run anywhere from four to seven years before the batteries need to be replaced.

Enabled by Texas Instruments' nano-power amplifiers, comparators, and the SimpleLink ultra-low-power wireless MCU platform, the Low-Power PIR Motion Detector With Sub-1GHz Wireless Connectivity Enabling 10-Year Coin Cell Battery Life TI Design demonstrates a motion detector circuit solution requiring no wiring while also fully maximizing the battery life.

At a high level, this TI Design consists of a CR2032 coin cell battery, two nano-power op amps, two nano-power comparators, an ultra-low-power wireless MCU, and a PIR sensor with analog signal output. The two op amps form an amplified bandpass filter with a high input impedance, which allows it to be connected directly to the sensor without loading it. The two comparators form a window comparator, which is used to compare the amplified sensor output to fixed reference thresholds so that motion can be distinguished from noise. The two outputs of the window comparator then serve as interrupts to the wireless MCU so that the MCU can operate in its lowest power sleep mode during times where there is no motion being detected and only wakes up to send messages back to a remote host when motion has been detected. Due to the nano-amp operation of the analog signal chain components, this TI Design achieves a 10-year battery life from a single CR2032 coin cell battery.

This design guide addresses component selection, design theory, and the testing results of this TI Design system. The scope of this design guide gives system designers a head-start in integrating TI’s nano-power analog components, and the SimpleLink ultra-low-power wireless MCU platform.

The following sub-sections describe the various blocks within the TI Design system and what characteristics are most critical to best implement the corresponding function.

2.1 Operational Amplifiers

In this TI Design, it is necessary to amplify and filter the signal at the output of the PIR sensor so that the signal amplitudes going into following stages in the signal chain are large enough to provide useful information.

Typical signal levels at the output of a PIR sensor are in the micro-volt range for motion of distant objects which exemplifies the need for amplification. The filtering function is necessary to primarily limit the noise bandwidth of the system before reaching the input to the window comparator. Secondarily, the filtering function also serves to set limits for the minimum and maximum speed at which the system will detect movement.

For an extremely long battery life, this TI Design uses the LPV802 because of its low current consumption of 320 nA (typical) per amplifier. Other considerations that make the LPV802 ideal for this TI Design are its low input voltage offset and low input bias current, which allows use of high value resistors, and rail-to-rail operation on both input and output. Additionally, the LPV802 integrates EMI protection to reduce sensitivity to unwanted RF signals, which is useful for low-power designs because of their high impedance nodes.

2.2 Comparators

In this TI Design, it is necessary to convert the amplified and filtered version of the sensor output into digital signals, which can be used as inputs to the MCU. To accomplish this, a window comparator circuit is used.

The low current consumption of only 75 nA (typical) per comparator makes the TLV3691 in this TI Design ideal. Other considerations for the comparator in this reference design include its low input voltage offset and low input bias current. Additionally, the TLV3691 features a rail-to-rail input stage with an input common mode range, which exceeds the supply rails by 100 mV, thereby preventing output phase inversion when the voltage at the input pins exceed the supply. This translates not only into robustness to supply noise, but also maximizes the flexibility in adjusting the window comparator thresholds in this design.

2.3 Ultra-Low-Power Wireless MCU

In this TI Design, transmitting the sensor information to some central location for processing is necessary. However, because power consumption is always a concern in battery-based applications, the radio and processor must be low power. Also, the wireless protocol required for the end-equipment system is an important consideration for the selection of the radio device.

With TI’s SimpleLink ultra-low-power wireless MCU platform, low power with a combined radio and MCU enables an extremely long battery life for sensor end-nodes. Furthermore, the CC1310 is a multi-standard device with software stack support for wM-Bus and IEEE 802.15.4g. In this TI Design, a generic sub-1GHz network protocol is the protocol of choice, but the hardware as built can work with other protocols as well.

2.4 Coin Cell Battery

The power source for this TI Design is a CR2032 lithium-ion coin cell. The selection of the CR2032 coin cell battery as the power source was due to the ubiquity of that battery type, particularly in small form factor systems such as a sensor end-node.

The voltage characteristics of a lithium-ion CR2032 coin cell battery are also ideal. The output voltage remains relatively flat throughout the discharge life until the cell is nearly depleted. When the cell is depleted, the output voltage drops off relatively quickly.

The temperature characteristics of lithium-ion batteries are also superior to that of alkaline cells, particularly at lower temperatures. This superiority is due to lithium-ion cells having a non-aqueous electrolyte that performs better than aqueous electrolytes commonly found in alkaline batteries. However, the CR2032 coin cell battery is still the limiting component in terms of the operating temperature range; all of the integrated circuits and other electrical components are specified to operate at a wider temperature range than the battery. Therefore, the specified operating temperature range of the TI Design system is −30°C to 60°C. Given an appropriate weather-proof enclosure, this TI Design system is suited for both indoor and outdoor use.

Immediately following the battery is a low R_{DS_ON} P-channel MOSFET and a bulk capacitor. The P-channel MOSFET prevents damage to the hardware if the coin cell battery is inserted backwards while minimizing the forward voltage drop in normal operation. The bulk capacitor is sized to prevent too much voltage droop, particularly during the transitions into the MCU on-state for radio transmissions.

2.5 PIR Sensor

The sensor chosen for the TI Design is the Murata IRS-B210ST01 PIR sensor. The choice of this sensor was due to the fact that it is in a surface mount package and provides an analog output so that the low-power circuit in this TI Design could be demonstrated in an area efficient footprint.

While the test results collected for this TI Design are focused on a particular PIR sensor part number, it is expected that similar results can be obtained with any similarly specified PIR sensor that is available when the techniques and circuit designs demonstrated in this TI Design are applied.

Lastly, for any PIR sensor, it is necessary to use a lens in front of the sensor to extend the detection range by focusing the infrared energy onto the sensor elements. Using a Fresnel lens, the infrared image for the viewing area is spread across all of the sensor elements. The lens shape and size, therefore, determines the overall detection angle and viewing area. For this TI Design, the Murata IML-0669 lens is used so that a maximum field of view and detection range could be demonstrated. Ultimately, the choice of lens will be determined by the field of view angle and detection range required by the application.

3 Block Diagram

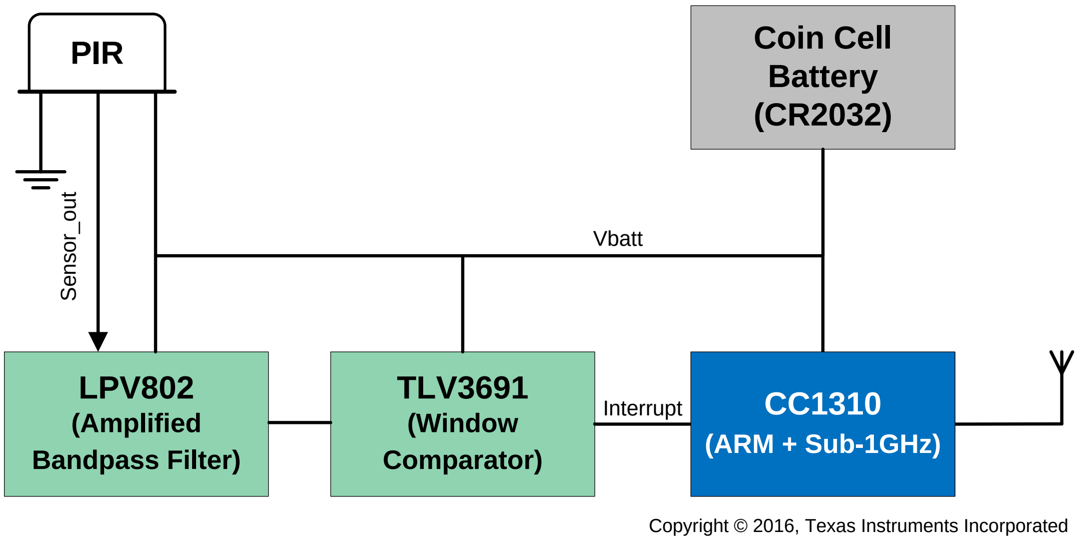

Figure 1. Wireless PIR System Block Diagram

3.1 *Highlighted Products*

The Low-Power PIR Motion Detector reference design features the following devices:

- LPV802 (Section 3.1.1): NanoPower, CMOS input, rail-to-rail IO operational amplifier
- TLV3691 (Section 3.1.2): NanoPower, CMOS input, rail-to-rail input comparator
- CC1310 (Section 3.1.3): SimpleLink multi-standard sub-1GHz ultra-low-power wireless MCU

For more information on each of these devices, see their respective product folders at www.ti.com.

3.1.1 LPV802

Features:

- For V_S = 3.3 V, typical unless otherwise noted
  - Supply current at 320 nA
  - Operating voltage range: 1.6 to 5.5 V
  - Low TCV_{OS} 1 µV/°C
  - V_{OS} 3.5 mV (max)
  - Input bias current: 100 fA
  - PSRR: 115 dB
  - CMRR: 98 dB
  - Open-loop gain: 120 dB
  - Gain bandwidth product: 8 kHz
  - Slew rate: 2 V/ms
  - Input voltage noise at f = 100 Hz 340 nV/√Hz
  - Temperature range: −40°C to 125°C

Applications:

- Gas Detectors (CO and O2)
- PIR Motion Detectors
- Ionization Smoke Detectors
- Thermostats
- IoT Remote Sensors
- Active RFID readers and Tags
- Portable Medical Equipment
- Sensor network powered by energy scavenging

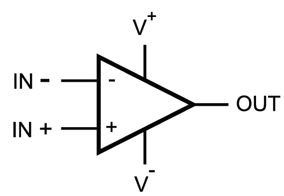

Figure 2. LPV802 Functional Block Diagram

The LPV802 is a dual nano-poweramplifier designed for ultra-long life battery applications. The operating voltage range of 1.6 V to 5.5 V coupled with typically 320 nA of supply current per channel make it well suited for remote sensor applications. The LPV802 has a carefully designed CMOS input stage that outperforms competitors with typically 100 fA I_{BIAS} currents and CMRR of 98 dB. This low input current significantly reduces I_{BIAS} and I_{OS} errors introduced in megohm resistance, high impedance photodiode, and charge sense situations. The LPV802 is a member of the PowerWise™ family and has an exceptional power-to-performance ratio.

EMI protection was designed into the device to reduce sensitivity to unwanted RF signals.

The LPV802 is offered in the 8-pin VSSOP 3.00 mm × 3.00 mm package.

3.1.2 TLV3691

Features:

- Low quiescent current: 75 nA
- Wide supply:
  - 0.9 to 6.5 V
  - ±0.45 to ±3.25 V
- Micro packages: DFN-6 (1 × 1 mm), 5-pin SC70
- Input common-mode range extends 100 mV beyond both rails
- Response time: 24 µs
- Low input offset voltage: ±3 mV
- Push-pull output
- Industrial temperature range: –40°C to 125°C

Applications:

- Overvoltage and undervoltage detection
- Window comparators
- Overcurrent detection
- Zero-crossing detection
- System monitoring:
  - Smart phones
  - Tablets
  - Industrial sensors
  - Portable medical

The TLV3691 offers a wide supply range, low quiescent current 150 nA (maximum), and rail-to-rail inputs. All of these features come in industry-standard and extremely small packages, making this device an excellent choice for low-voltage and low-power applications for portable electronics and industrial systems.

Available as a single channel, the low-power, wide supply, and temperature range makes this device flexible enough to handle almost any application from consumer to industrial. The TLV3691 is available in SC70-5 and 1×1-mm DFN-6 packages. This device is specified for operation across the expanded industrial temperature range of –40°C to 125°C.

3.1.3 CC1310

Features:

- MCU:
  – Powerful ARM® Cortex®-M3
  – EEMBC CoreMark® score: 142
  – EEMBC ULPBench™ score: 158
  – Up to 48-MHz clock speed
  – 128KB of in-system programmable Flash
  – 8KB of SRAM for cache (or as general-purpose RAM)
  – 20 KB of ultra-low leakage SRAM
  – 2-pin cJTAG and JTAG debugging
  – Supports over-the-air (OTA) upgrade
- Ultra-low-power sensor controller:
  – Can run autonomous from the rest of the system
  – 16-bit architecture
  – 2KB of ultra-low leakage SRAM for code and data
- Efficient code-size architecture, placing TI-RTOS, drivers, *Bluetooth*® Low Energy Controller, IEEE 802.15.4 MAC, and Bootloader in ROM
- RoHS-compliant package:
  – 7×7-mm RGZ VQFN48 (30 GPIOs)
  – 5×5-mm RHB VQFN48 (15 GPIOs)
  – 4×4-mm RSM VQFN48 (10 GPIOs)
- Peripherals:
  – All digital peripheral pins can be routed to any GPIO
  – Four general-purpose timer modules (Eight 16-bit or four 32-bit timers, PWM each)
  – 12-bit ADC, 200 ksps, 8-channel analog MUX
  – Continuous time comparator
  – Ultra-low-power clocked comparator
  – Programmable current source
  – UART
  – 2× SSI (SPI, MICROWIRE, TI)
  – I^2C
  – I^2S
  – Real-time clock (RTC)
  – AES-128 security module
  – True random number generator (TRNG)
  – Support for eight capacitive sensing buttons
  – Integrated temperature sensor
- External system:
  – On-chip internal DC-DC converter
  – Very few external components
  – Seamless integration with the SimpleLink CC1190 range extender

- Low power:
  - Wide supply voltage range: 1.8 to 3.8 V
  - Active-Mode RX: 5.5 mA
  - Active-Mode TX at 10 dBm: 12.9 mA
  - Active-mode MCU 48 MHz running CoreMark: 2.5 mA (51 µA/MHz)
  - Active-mode MCU: 48.5 CoreMark/mA
  - Active-mode sensor controller at 24 MHz: 0.4 mA + 8.2 µA/MHz
  - Sensor controller, one wake up every second performing one 12-bit ADC sampling: 0.85 µA
  - Standby: 0.6 µA (RTC running and RAM and CPU retention)
  - Shutdown: 185 nA (wakeup on external events)
- RF section:
  - 2.4-GHz RF transceiver compatible with *Bluetooth* Low Energy (BLE) 4.1 specification and IEEE 802.15.4 PHY and MAC
  - Excellent receiver sensitivity –124 dBm using long-range mode, –110 dBm at 50 kbps, –89 dBm at BLE
  - Excellent selectivity: 52 dB
  - Excellent blocking performance: 90 dB
  - Programmable output power up to 14 dBm
  - Single-ended or differential RF interface
  - Suitable for systems targeting compliance with worldwide radio frequency regulations:
    - ETSI EN 300 220, EN 303 131, EN 303 204 (Europe)
    - EN 300 440 Class 2 (Europe)
    - FCC CFR47 Part 15 (US)
    - ARIB STD-T108 (Japan)
  - Wireless M-Bus and IEEE 802.15.4g PHY
- Tools and development environment:
  - Full-feature and low-cost development kits
  - Multiple Reference Designs for Different RF Configurations
  - Packet sniffer PC software
  - Sensor Controller Studio
  - SmartRF™ Studio
  - SmartRF Flash Programmer 2
  - IAR Embedded Workbench® for ARM
  - Code Composer Studio™

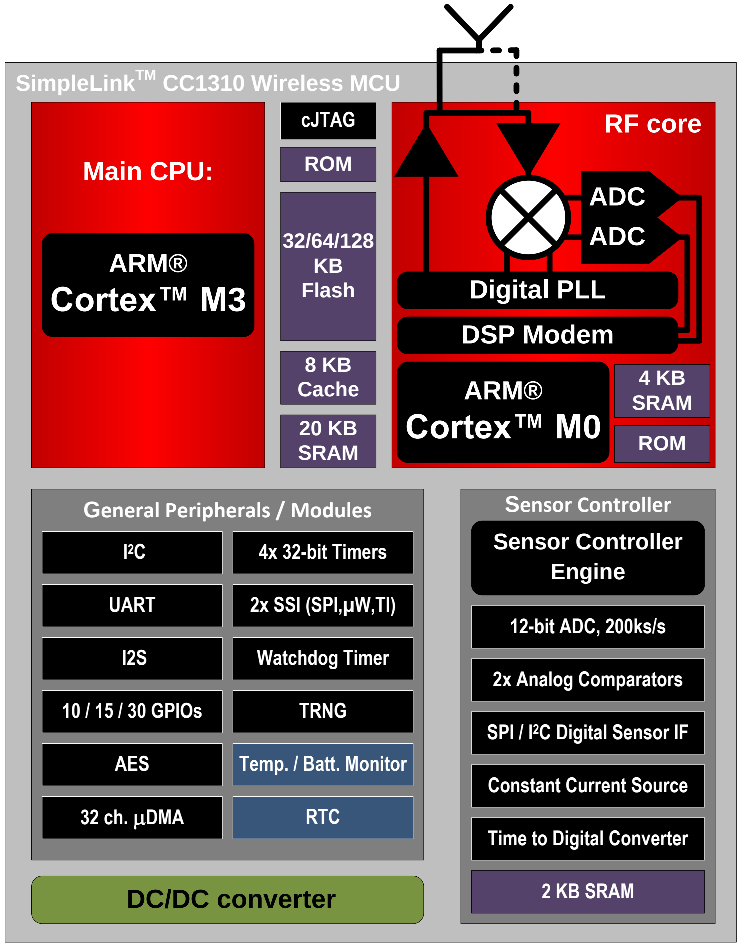

Figure 3. CC1310 Functional Block Diagram

This device is a member of the CC26xx and CC13xx family of cost-effective, ultra-low-power, 2.4-GHz and sub-1GHz RF devices. Very low active RF, MCU current, and low-power mode current consumption provide excellent battery lifetime and allow operation on small coin-cell batteries and in energy-harvesting applications.

The CC1310 is the first part in a Sub-1GHz family of cost-effective, ultra-low-power wireless MCUs. The CC1310 device combines a flexible, very low-power RF transceiver with a powerful 48-MHz Cortex-M3 MCU in a platform supporting multiple physical layers and RF standards. A dedicated radio controller (Cortex-M0) handles low-level RF protocol commands that are stored in ROM or RAM, thus ensuring ultra-low power and flexibility. The low-power consumption of the CC1310 does not come at the expense of RF performance; the CC1310 has excellent sensitivity and robustness (selectivity and blocking) performance.

The CC1310 is a highly integrated, true single-chip solution incorporating a complete RF system and an on-chip DC-DC converter.

Sensors can be handled in a very low-power manner by a dedicated autonomous ultra-low-power MCU that can be configured to handle analog and digital sensors; thus the main MCU (Cortex-M3) is able to maximize sleep time.

The CC1310 power and clock management and radio systems require specific configuration and handling by software to operate correctly. This has been implemented in the TI RTOS, and it is therefore recommended that this software framework is used for all application development on the device. The complete TI-RTOS and device drivers are offered in source code free of charge.

4 System Design Theory

The Low-Power PIR Motion Detector With Sub-1GHz Wireless Connectivity Reference Design senses motion by detecting differences in infrared (IR) energy in the field of view of the sensor. Because the sensor output is a very small signal, amplification and filtering are necessary to boost the signal and at the same time filter noise so that a representation of the sensor output at a reasonable signal level is obtained while also minimizing false trigger events. The scaled analog output is then converted to digital signals by a window comparator function whose outputs can be used as interrupts to the wireless MCU to save power by only waking up the MCU when it is needed. The following sections discuss the details of the design for these different circuit sections that make up the design's overall sub-system.

4.1 PIR Sensor

To better understand the circuit, the user must understand how the PIR motion sensor operates. The PIR motion sensor consists of two or more elements that output a voltage proportional to the amount of incident infrared radiation. Each pair of pyroelectric elements are connected in series such that if the voltage generated by each element is equal, as in the case of IR due to ambient room temperature or no motion, then the overall voltage of the sensor elements is 0 V. Figure 4 shows an illustration of the PIR motion sensor construction.

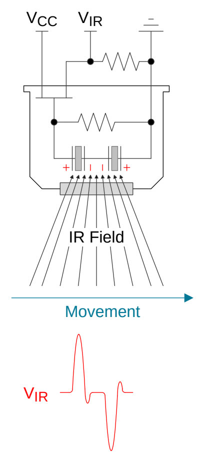

Figure 4. PIR Motion Sensor Illustration

The lower part of Figure 4 shows the output voltage signal resulting from movement of a body with a different temperature than the ambient parallel to the surface of the sensor and through the field of view of both sensor elements. The amplitude of this signal is proportional to the speed and distance of the object relative to the sensor and is in a range of low millivolts peak to peak to a few hundred microvolts peak to peak or less. A JFET transistor is used as a voltage buffer and provides a DC offset at the sensor output.

Because of the small physical size of the sensor elements, a Fresnel lens is typically placed in front of the PIR sensor to extend the range as well as expanding the field of view by multiplying and focusing the IR energy onto the small sensor elements. In this manner, the shape and size of the lens determine the overall detection angle and viewing area. The style of lens is typically chosen based on the application and choice of sensor placement in the environment. Based on this information, for best results, the sensor should be placed so that movement is across the sensor instead of straight into the sensor and away from sources of high or variable heat such as AC vents and lamps.

Also note that on initial power up of the sensor, it takes up to 30 s or more for the sensor output to stabilize. During this "warm up" time, the sensor elements are adjusting themselves to the ambient background conditions. This is a key realization in designing this subsystem for maximum battery life in that the sensor itself must be continuously powered for proper operation, which means power cycling techniques applied to either the sensor or the analog signal path itself cannot be applied for proper operation and reliable detection of motion.

4.2 Analog Signal Path

The analog signal conditioning section is shown in the schematic in Figure 5. The first two stages in Figure 5 implement the amplified filter function whereas stage 3 implements the window comparator design. Components R10 and C5 serve as a low pass filter to stabilize the supply voltage at the input to the sensor and are discussed further in Section 4.3.

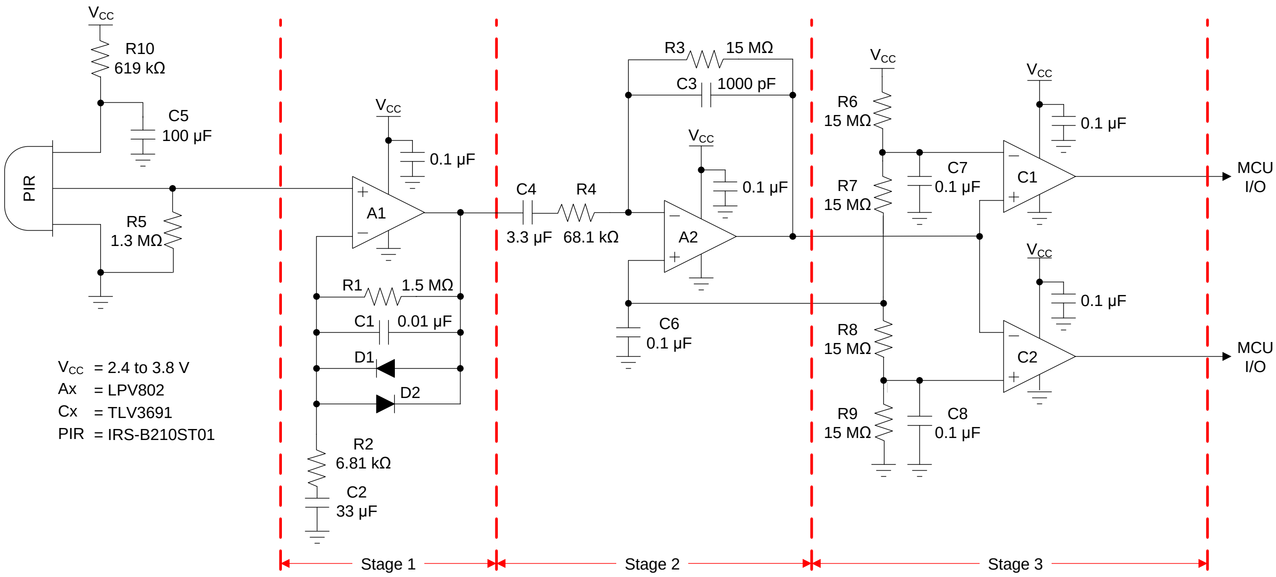

Figure 5. PIR Motion Sensor Analog Signal Path Schematic

Resistor R5 sets the bias current in the JFET output transistor of the PIR motion sensor. To save power, R5 is larger than recommended and essentially current starves the sensor. This comes at the expense of decreased sensitivity and higher output noise at the sensor output, which is a fair tradeoff for increased battery lifetime. Some of the loss in sensitivity at the sensor output can be compensated by a gain increase in the filter stages. Due to the higher gain in the filter stages and higher output noise from the sensor, carefully optimize the placement of the high frequency filter pole and the window comparator thresholds to avoid false detection.

4.2.1 Amplified Filter Design

Composed of stages 1 and 2 in Figure 5, the filter section implements a fourth order bandpass filter using simple poles. Each stage implements identical second order bandpass filter characteristics. The chosen cutoff frequencies for the bandpass filter are set to 0.7 and 10.6 Hz. The passband gain of each stage is 220 for an overall signal gain of ~90 dB and was chosen to maximize the motion sensitivity range for the sensor bias point being used. The data collected for motion sensitivity range at different sensor bias and gain settings is shown in Section 8.3.1.

Generally, the filter bandwidth should be wide enough to detect a person walking or running by the sensor. At the same time, the filter bandwidth should be narrow to limit the peak-to-peak noise at the output of the filter. In most cases, a bandwidth between 0.3 to 2 Hz is acceptable for this application; however, the use of simple poles means the filter Q is low, which leads to a large filter transition region. With the poles placed this close, the overall passband gain is reduced, which reduces sensitivity and increases the noise floor.

The low frequency cutoff is critical because it has a major effect on the system noise floor by limiting the overall impact of 1/f noise from the analog front end as well as setting the minimum speed of motion that the system can detect. The practical lower limit on the low frequency cutoff is due to capacitor sizing at 0.1 Hz. Due to the low bias current being used in the sensor for this design, the low frequency noise will be worse than a normal higher current design, which means the low frequency cutoff should be higher than 0.3 Hz. Given a practical range of the low frequency cutoff to be between 0.3 to 1 Hz, this design used a low frequency cutoff in the middle of this range.

The high frequency cutoff is mostly for reducing broadband noise. The range for its placement will be a decade higher than the low frequency cutoff up to the bandwidth limit set by the open loop bandwidth of the op amp being used. In this case, the LPV802 has a unity gain bandwidth (UGBW) of 8 kHz, which means for a maximum stage gain of 220, the bandwidth is limited to 36 Hz. Allowing for component tolerances and variation in the UGBW of the LPV802, a practical range for the high frequency cutoff is between 7 and 14 Hz. Again, the choice was made to use a high frequency cutoff in the middle of this range.

The first stage of the filter is arranged as a non-inverting gain stage. This provides a high impedance load to the sensor so its bias point remains fixed. Because this stage has an effective DC gain of one due to C2, the sensor output bias voltage provides the DC bias for the first filter stage. Feedback diodes, D1 and D2 provide clamping so that the op amps in both filter stages stay out of saturation for motion events which are close to the sensor. Equation 1 to Equation 3 show the gain and cutoff frequencies for this stage:

$$f_{Low1} = \frac{1}{2\pi \times R2 \times C2} = \frac{1}{2\pi \times 6.81\,k\Omega \times 33\,\mu F} = 0.71\,Hz \tag{1}$$

$$f_{High1} = \frac{1}{2\pi \times R1 \times C1} = \frac{1}{2\pi \times 1.5\,M\Omega \times 0.01\,\mu F} = 10.6\,Hz \tag{2}$$

$$|G_1| = 1 + \frac{R1}{R2} = 1 + \frac{1.5\,M\Omega}{6.81\,k\Omega} = 221.26 \tag{3}$$

Since the second stage is AC coupled to the first stage, it is arranged as an inverting gain stage. This allows the DC bias to be set to $V_{CC}/2$ easily by connecting the center point of the divider string in the window comparator to the non-inverting input of the op amp in this filter stage. Because the peak-to-peak noise is present at the output of this stage, R3 is made as large as possible to minimize the dynamic current of the system. Equation 4 to Equation 6 show the gain and cutoff frequencies for this stage:

$$f_{Low2} = \frac{1}{2\pi \times R4 \times C4} = \frac{1}{2\pi \times 68.1\,k\Omega \times 3.3\,\mu F} = 0.71\,Hz \tag{4}$$

$$f_{High2} = \frac{1}{2\pi \times R3 \times C3} = \frac{1}{2\pi \times 15\,M\Omega \times 1000\,pF} = 10.6\,Hz \tag{5}$$

$$|G_2| = \left|-\frac{R3}{R4}\right| = \left|-\frac{15\,M\Omega}{68.1\,k\Omega}\right| = 220.26 \tag{6}$$

The total circuit gain (not including any gain reduction due to pole placement), is given by G1 × G2 = 221.26 × 220.26 = 48810 = 93.77 dB. Figure 6 and Figure 7 show simulation results for these two filter stages.

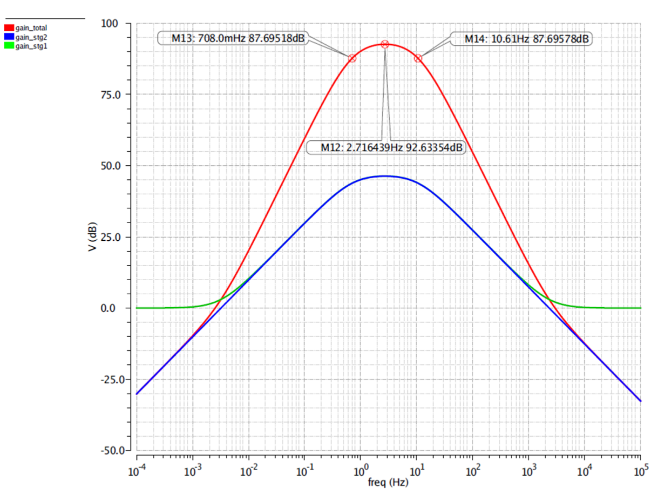

Figure 6. Amplified Filter Simulation Results (Ideal)

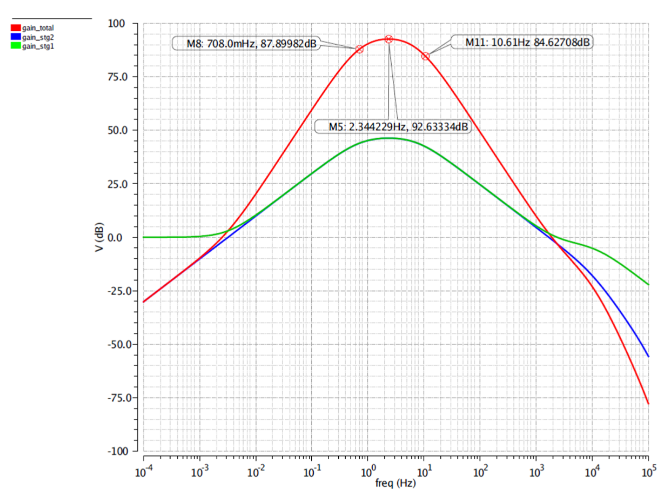

Figure 7. Amplified Filter Simulation Results (Nonideal)

The responses shown in Figure 6 and Figure 7 illustrate the effect of finite unity gain bandwidth for the amplifiers in the circuit. Note that not only is the high frequency response altered, but also the attenuation at the high frequency cutoff is increased and the peak gain frequency is shifted slightly.

4.2.2 Window Comparator Design

The window comparator circuit shown in stage 3 of Figure 5 converts the analog output of the filter to digital signals, which are used as interrupts to the MCU to tell it when motion has been detected. Composed of resistors R6 through R9, the resistor divider sets up the thresholds that determine a valid motion detection from the sensor. To save power, this resistor divider also provides the bias voltage for the second stage of the filter. Capacitors C6, C7, and C8 are necessary to stabilize the threshold voltages to prevent chatter at the output of the comparators. These capacitors do not need to be a large value due to the large resistors being used in the resistor divider, but they should be low ESR and low leakage, with ceramic being preferred. The comparator chosen for this reference design is the TLV3691 due to its ultra-low supply current requirements. The TLV3691 comparator also has rail-to-rail input capability with an input common mode range that exceeds the supply rails by 100 mV. This is not required for this design, but it does allow the ability to maximize the adjustment range of the window comparator thresholds. The comparator outputs will be low when there is no motion detected. Typically, motion across the sensor will generate a high pulse on one comparator output followed by a high pulse on the other comparator, which corresponds to the amplification of the S-curve waveform shown in the lower part of Figure 4. Which comparator triggers first will depend on the direction of the motion being detected.

Equation 7 and Equation 8 are used to adjust the window comparator thresholds:

$$V_{REF\_High} = V_{CC}\frac{R7 + R8 + R9}{R6 + R7 + R8 + R9} = 0.75 \times V_{CC} \quad (7)$$

$$V_{REF\_Low} = V_{CC}\frac{R9}{R6 + R7 + R8 + R9} = 0.25 \times V_{CC} \quad (8)$$

There is also a constraint that R6 + R7 = R8 + R9 so that the $V_{CC}/2$ bias level is maintained at the center tap of the divider for use as the bias for the second stage of the filter.

The thresholds chosen for this design are a balance between sensitivity and noise immunity. Widening of the window improves noise immunity but reduces sensitivity. Making the window too small can lead to false triggers due to the peak-to-peak noise seen at the input to the window comparator.

4.3 Power Supply Design

Because of the increasing battery impedance over the life of the battery supply and the low power supply rejection of the PIR sensor, it is important to design the power supply network to prevent current spikes generated by the MCU from causing false triggers through the analog signal path. While the algorithm implemented in firmware helps to filter such problems, this unwanted power supply feedback loop can become an issue. Ideally, the sensor supply would be regulated to break this loop; however, in this design the extra quiescent current of a regulator would reduce battery life, so other methods were explored.

Figure 8 shows a simplified schematic of the power supply network. The PMOS transistor is used in place of the traditional Schottky diode for reversed battery protection. Because the peak currents are in the 30-mA range when the radio transmits, using a low R_{DS_ON} PMOS provides a much lower voltage drop compared to a Schottky diode, which helps to maximize battery life by allowing the battery to decay to a lower voltage before the circuit is no longer able to function (for more on this technique, see SLVA139).

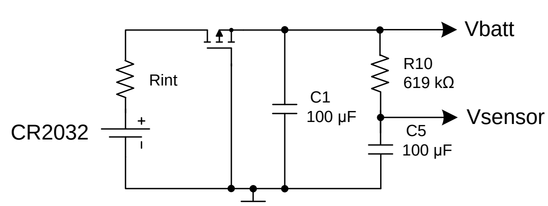

Figure 8. PIR Motion Sensor Simplified Power Supply Network Schematic

Capacitor C1 supplies the circuit during periods of high and fast peak current demand, which helps to maximize the battery capacity and minimize voltage droop on the power supply rail, especially as the battery approaches its end of life and its internal impedance increases (represented by Rint in Figure 8). The calculation for C1 is provided in Equation 9. For more details on this calculation and the effects of high current peaks on battery life and capacity, see White Paper SWRA349.

$$C1 = \frac{\Delta Q}{V_{MAX} - V_{MIN}} \tag{9}$$

where

- $\Delta Q = Q_{dis} - \frac{V_{MIN}}{Rint} t_{tot}$
- $Q_{dis} = \sum i_n \times t_n$

V_{MAX} is the voltage across the capacitor at the start of the current pulse at the end of the battery's life, and V_{MIN} is the circuit operating minimum, which is the sensor minimum plus the voltage drop across R10 due to the sensor bias current (2 V + 0.6 µA × 619 kΩ ~ 2.4 V). V_{MAX} is taken to be 2.698 V assuming an unloaded end of life battery voltage of 2.7 V (V_P). Based on the measured current profile during a radio transmission, shown in Figure 22 and Figure 23:

$$Q_{dis} = 23.2\ \text{mA} \times 100\ \mu\text{s} + 4\ \text{mA} \times 3.5\ \text{ms} + 8.8\ \text{mA} \times 2.5\ \text{ms} = 38.32\ \mu\text{C} \tag{10}$$

For C1:

$$C1 = \frac{38.32\ \mu\text{C} - \frac{2.4\ \text{V}}{1\ \text{k}\Omega} \times 6.1\ \text{ms}}{2.698\ \text{V} - 2.4\ \text{V}} = 79.5\ \mu\text{F} \tag{11}$$

This design uses C1 = 100 µF and additional decades of capacitors in parallel for improved impedance at higher frequencies. The time required to recharge the composite C1 capacitor after the high current event is given in Equation 12 and is sufficiently low compared to the active and standby states of the device where current consumption is in the low microamp range.

$$t = Rint \times C1 \times \ln\left(\frac{V_p - V_{MIN}}{V_p - V_{MAX}}\right) = 1\ \text{k}\Omega \times 111.514\ \mu\text{F} \times \ln\left(\frac{2.7\ \text{V} - 2.4\ \text{V}}{2.7\ \text{V} - 2.698\ \text{V}}\right) = 0.56\ \text{s} \tag{12}$$

With the value of C1 determined, R10 and C5 can be sized to prevent false triggers from occurring during high current events on the power supply. With R10 chosen based on the acceptable amount of voltage drop due to the sensor bias, C5 was determined experimentally. If desired, R10 can be reduced in value to be able to operate at slightly lower voltage; however, the time constant for R10 and C5 shown in Figure 8 needs to be maintained. This means C5 becomes larger and would require a different dielectric, which in all likelihood would be more leaky or more costly and negate some of the advantage to reducing R10. Similar to what was done for C1, C5 has additional decades of capacitors in parallel to maintain a low impedance at higher frequencies.

4.4 Firmware Control

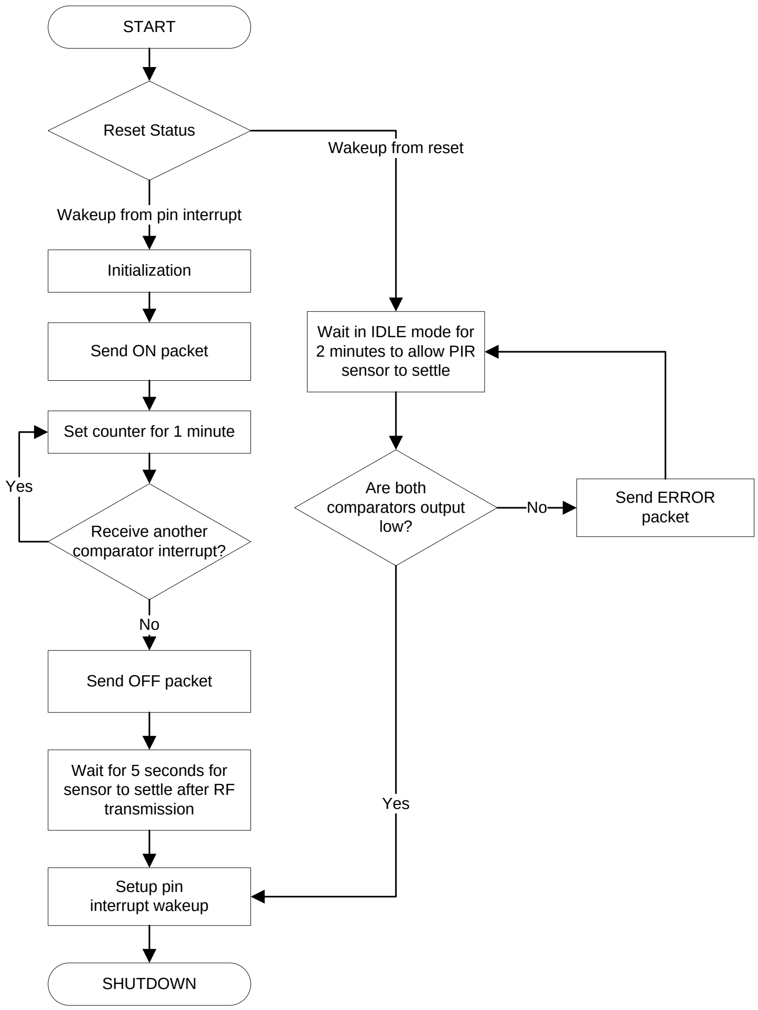

Figure 9. Wireless PIR Firmware Flowchart

The flowchart shown in Figure 9 describes the CC1310 operation in this TI Design. The CC1310 first starts by checking the source of wake up. If the device is woken up by reset, the system is powered on for the first time. The CC1310 will wait in standby mode for two minutes to allow the PIR sensor and analog signal chain to power on and allow the operating point to settle. After two minutes, the firmware will look at the outputs of the window comparator. By default, the output of both comparators should be low. If either comparator output is high, the CC1310 will send an ERROR message and will wait an additional amount of time for the sensor to settle. Once the PIR sensor and analog signal chain are functioning correctly, the CC1310 will enter shutdown mode.

The CC1310 will stay in shutdown mode until the PIR sensor signals the MCU that motion is detected by means of the window comparator outputs serving as interrupts. When the CC1310 is woken up by the PIR sensor, it will send an ON packet to notify the host controller that motion has been detected. The CC1310 will wait until the PIR sensor is silent for one minute before sending an OFF packet to the host controller and returning to shutdown mode.

5 Getting Started: Hardware

Figure 10 shows the hardware for the Low-Power PIR Motion Detector With Sub-1GHz Wireless Connectivity Enabling 10-Year Coin Cell Battery Life TI Design. The printed circuit board (PCB) is in a 35×75-mm rectangular form factor and comes with 0.5-in nylon standoffs to ensure ease of use while performing lab measurements.

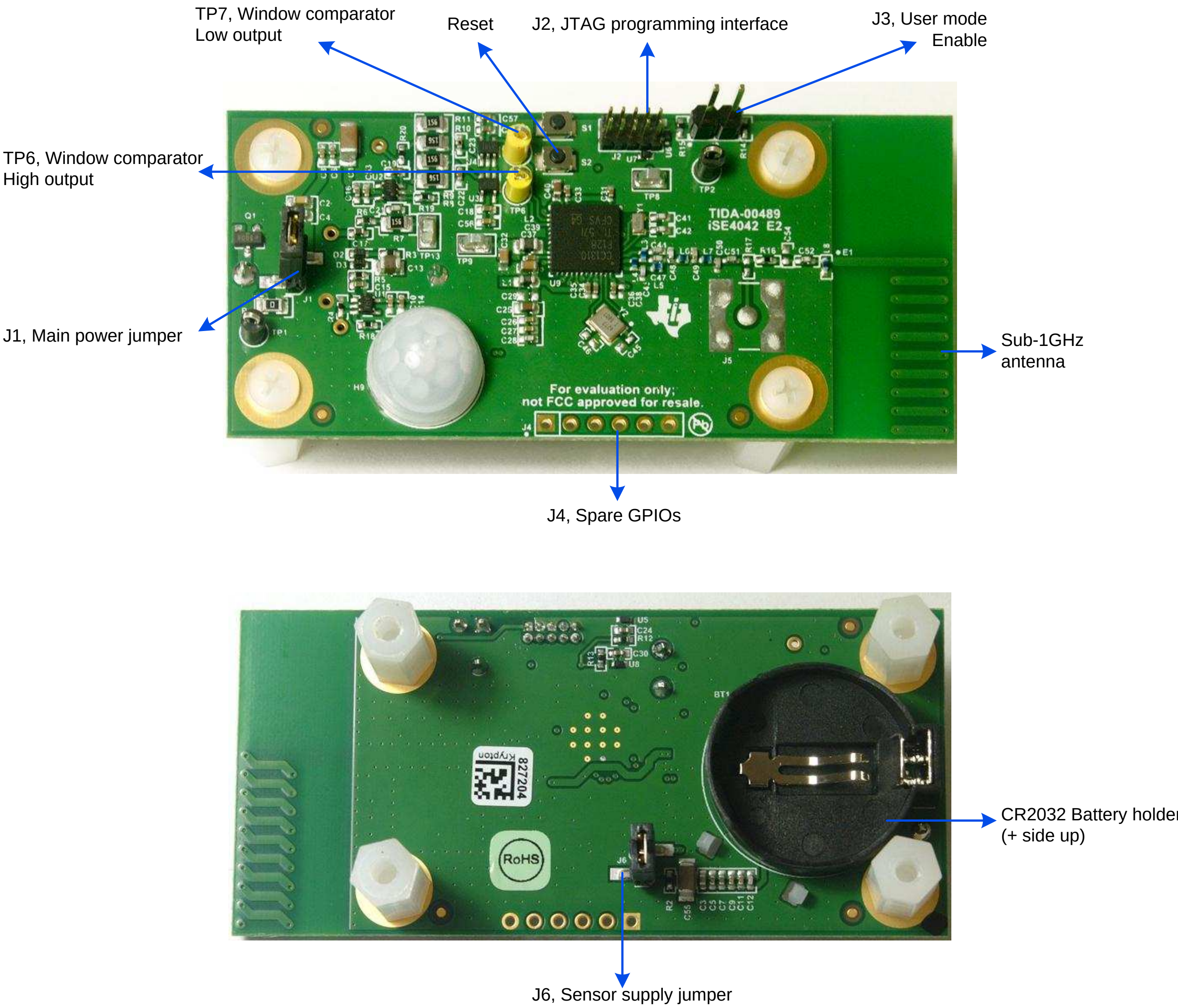

Figure 10. Low-Power Wireless PIR Motion Detector Reference Design Hardware Description

All the integrated circuits (CC1310, LPV802, and TLV3691), several test points, and jumpers are located on the top side of the PCB. The antenna is also located on the top side of the PCB.

The bottom side of the PCB contains the CR2032 coin cell battery holder, jumper J6, and the bottom half of the antenna.

There are four unused GPIOs that have been brought out from the CC1310 to an unpopulated header to facilitate future prototyping and debugging.

5.1 Jumper Configuration

To facilitate measuring critical parameters and debugging in this reference design, there are several jumpers included. However, to properly operate the design, these jumpers must be installed correctly. The jumper configuration for normal operation is as follows: J1 = Shorted, J2 = Open, J3 = Open, J6 = Shorted. The jumper configuration to program the CC1310 is as follows: J1 = Open (power applied to Pin 2), J2 = Connected through ribbon cable to the SmartRF06 Evaluation Board (EVM), J3 = Open, J6 = Don’t care.

See Figure 10 for a brief description of the intended function of these different jumpers.

5.2 Test Point Description

This design includes several test points to monitor critical signals. The following is a brief description of these test points:

- TP1, TP2: Ground points for probes or common points for voltage measurements
- TP6, TP7: Window comparator high threshold and low threshold outputs, respectively
- TP8: Filtered battery supply forming input to the DC-DC converter in the CC1310
- TP9: Filtered DC-DC converter output from the CC1310
- TP13: Output of analog filter stage, which is also the input to the window comparator stage

5.3 Miscellaneous

Note that due to the number of sensitive high impedance nodes in this design, probing points aside from the ones with dedicated test points should be done so with the probe impedance in mind.

An example of this would be the probing of the reference inputs to the window comparator. Because these reference thresholds are generated from a resistor divider composed of four 15-MΩ resistors, using a standard oscilloscope probe or voltmeter with a 10-MΩ input impedance will effectively load the circuit being measured and provide a false measurement.

6 Getting Started: Firmware

6.1 Loading Firmware

The firmware used on this TI Design was developed using TI's Code Composer Studio software (version 6.1.0).

The IAR Embedded Workbench for ARM also supports the CC13xx line of SimpleLink products.

Powering the board from 3.0 V is also necessary and is supplied at pin 2 of Jumper J1. Connecting the external power source at this location bypasses the reversed battery protection.

The TI Design hardware is programmed by connecting the 10-pin mini ribbon cable from J2 to the SmartRF06 EVM (10-pin ARM Cortex Debug Connector, P410). See Figure 11 for a photo of the correct setup for connecting the TI Designs hardware to the SmartRF06 EVM.

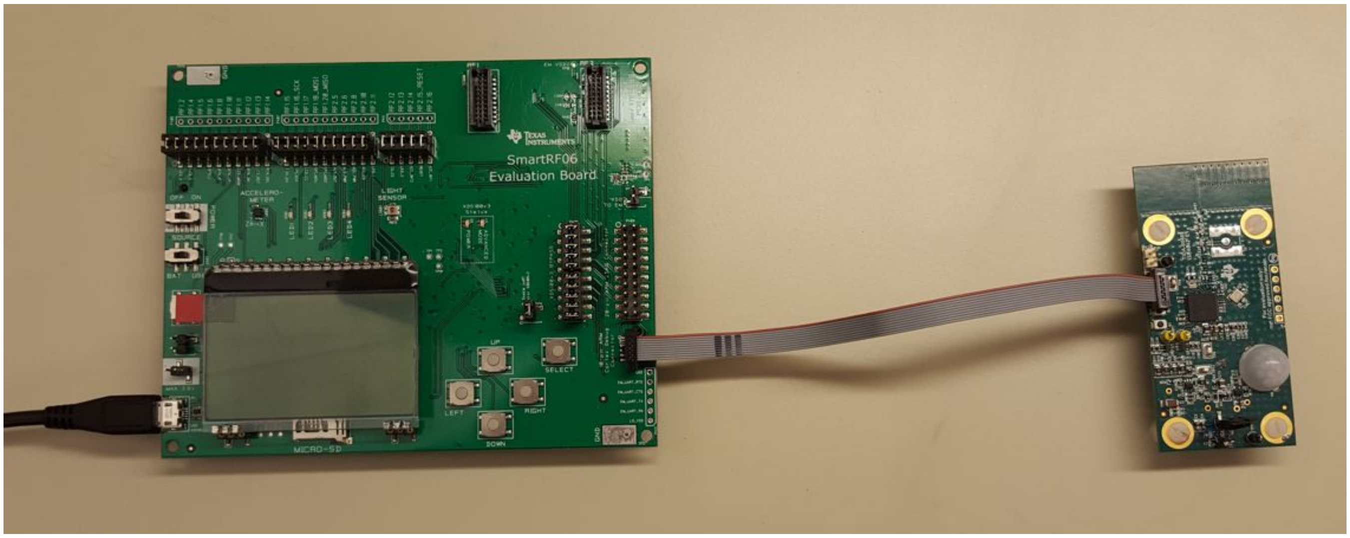

Figure 11. Connection of SmartRF06 Evaluation Board and TI Designs Hardware for Programming and Debugging

6.2 Receiving Data Packets

As this reference guide previously describes, this TI Design is programmed to detect a person's presence by using the PIR sensor (see Section 2.5 and Section 4.1). The CC1310 will broadcast three possible action values:

- 0xEE: Error during startup of the sensor
- 0xAA: ON packet when the first motion is detected
- 0xFF: OFF packet one minute after the last motion is detected

To verify the proper operation of the radio transmission, two methods to view the transmitted packet are described in the following subsections.

6.2.1 Building Automation Sub-1GHz Sniffer GUI

The first method is a Sniffer GUI firmware running on the SmartRF06 EVM with the CC13xxEM radio. The Sniffer GUI firmware will process the received packet and display the calculated data on the LCD screen.

As shown in Figure 12, the LCD screen will show the six most current received data. If more data is needed for testing or characterization purposes, Section 6.2.2 describes how to log more data samples for post analysis.

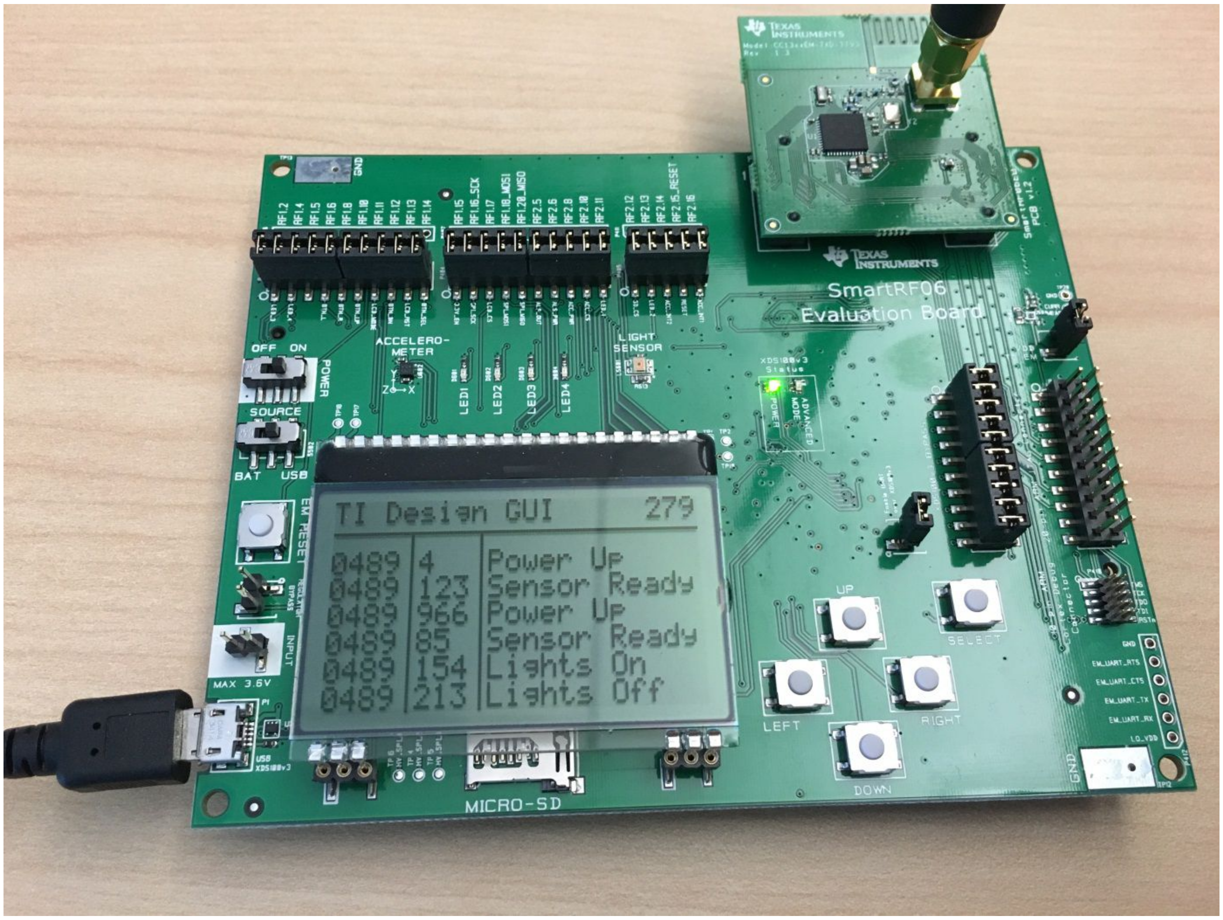

Figure 12. Building Automation Sub-1GHz Sniffer GUI

For more information about the Sniffer GUI, download and install the Building Automation Sub-1GHz Sniffer GUI software package that is available in Section 10.

6.2.2 CC1111 USB Dongle and SmartRF Protocol Packet

The second method uses the CC1111 USB dongle, CC1111 USB EVM Kit 868/915 MHz, to "sniff" packets using the SmartRF™ Protocol Packet Sniffer software. The data is displayed as raw data stream. This data stream can be post processed and be used for testing and characterization. After installing the packet sniffer software (v2.18.1 at the time of this writing), the procedure to detect the data transmissions is as follows:

1. Plug the CC1111 USB dongle into an unused USB port on the computer with the packet sniffer software installed.
2. Open the packet sniffer software. Choose Generic as the protocol, and click the Start button (see Figure 13).

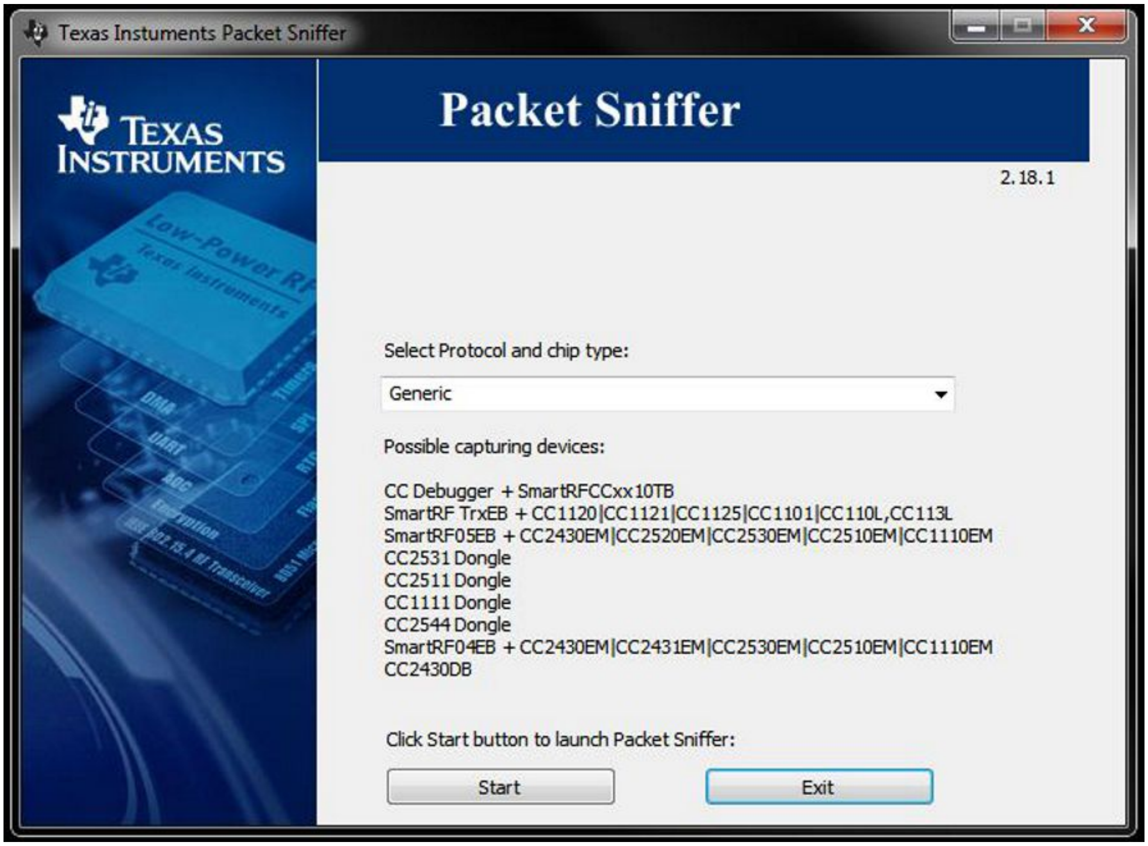

Figure 13. Packet Sniffer Software

3. Configure the CC1111 correctly to see the packets. Select the Radio Configuration tab. Under the Register settings sub tab, click on the "Browse…" button. Open the TIDA-00489_CC1111.prs file. Highlight and double-click on "TIDA-00489_CC1111" to apply the register settings (see Figure 14).

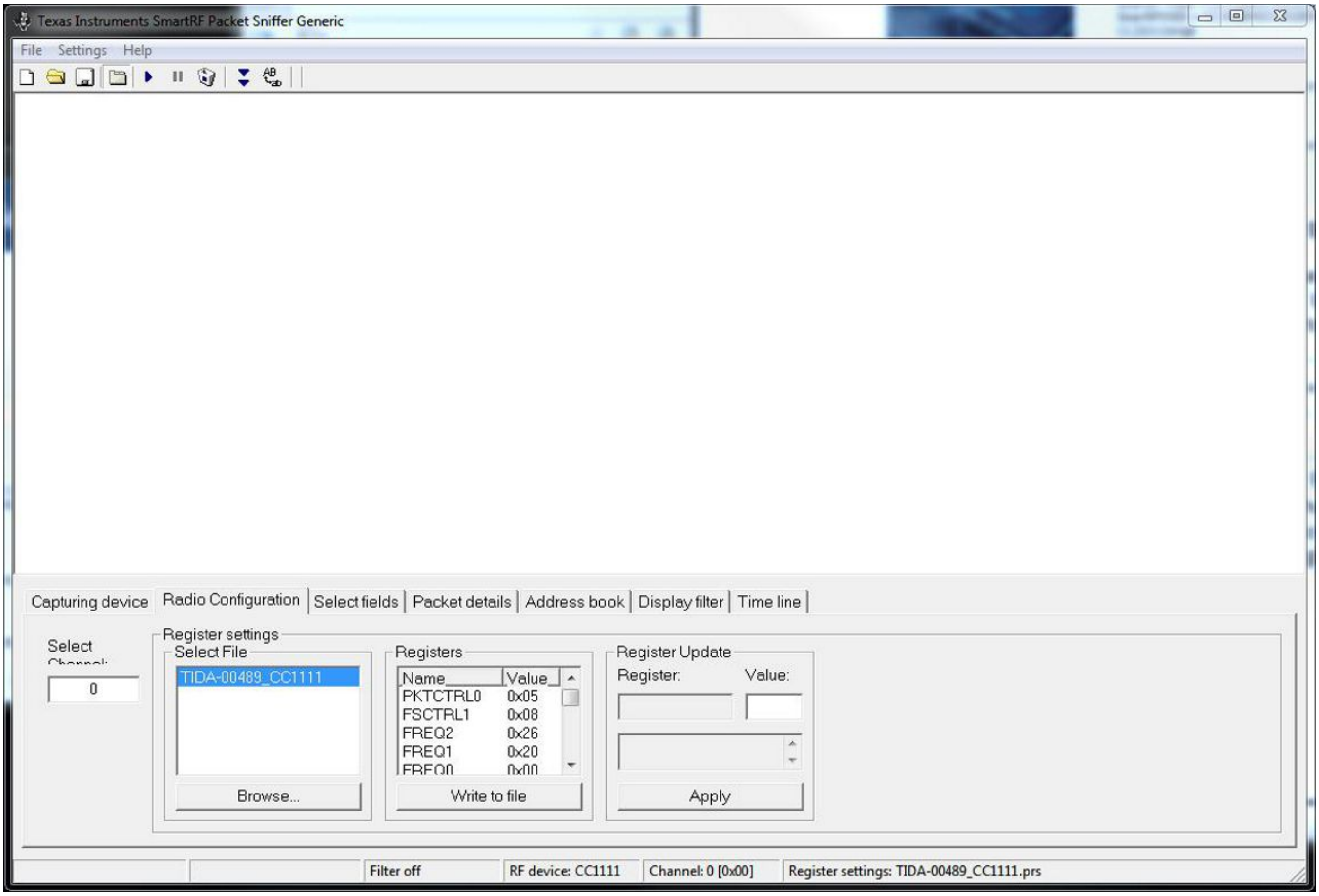

Figure 14. Packet Sniffer Software, Register Setting

NOTE: If long data acquisition periods are expected, increase the Cache Buffer size in the packet sniffer software to prevent possible crashes. Take this action by opening the Settings menu and clicking "Cache buffer size...".

---

4. Press the Play button on the top toolbar to initiate the packet capture process.

5. The packet sniffer software is likely to detect many other packets. To view only the valid data packets, apply a display filter. Figure 15 shows a sample display of what records without a filter applied. The highlighted row shows an undesired data packet.

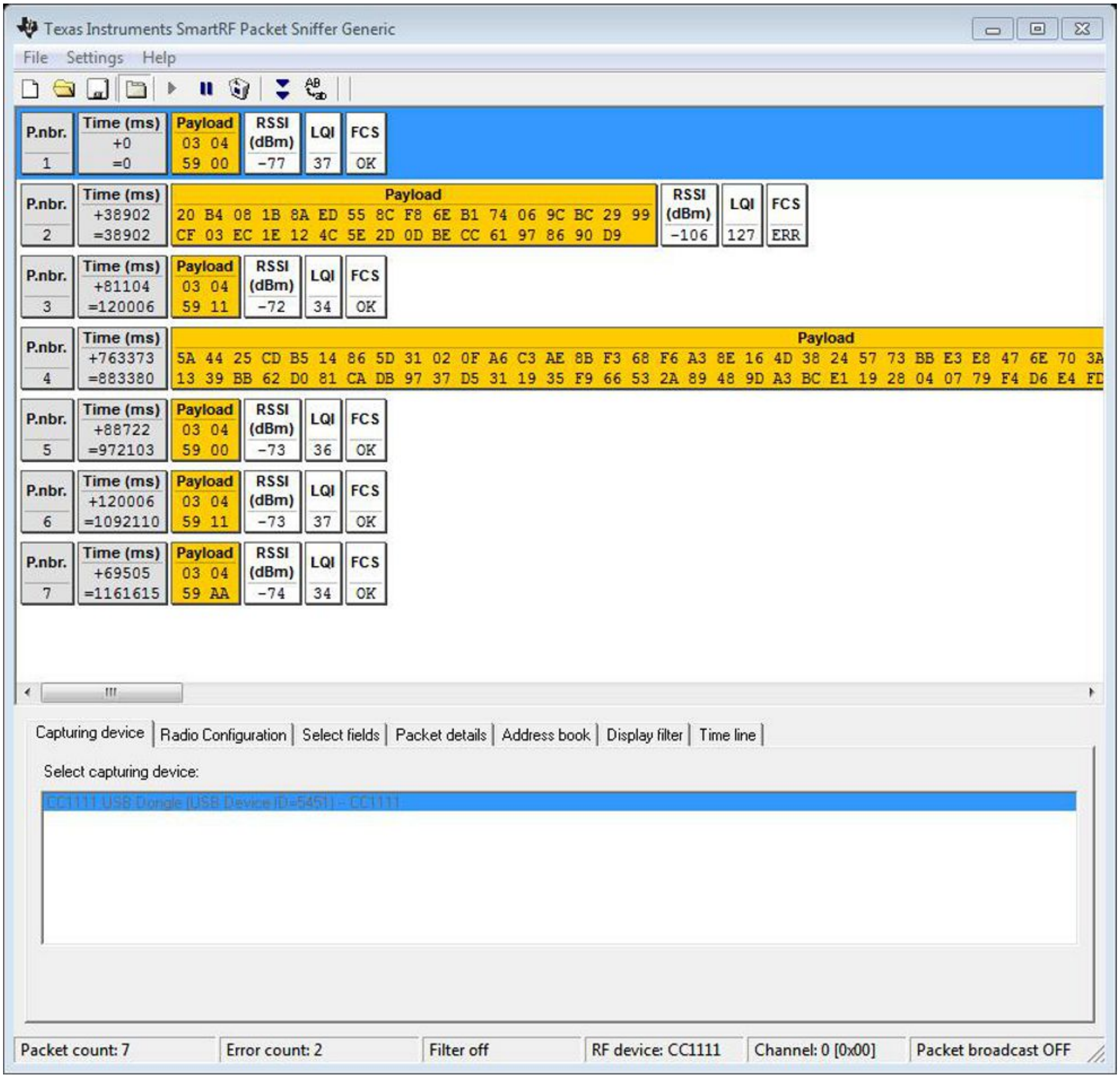

Figure 15. Packet Sniffer Software, Filterless Recording

6. To add the appropriate filter checks for only valid packets, select the Display filter tab. In the Field Name field, select "FCS" from the drop-down options. Click the button labeled First. Modify the filter condition to only show "OK" packets by typing "FCS=OK" in the Filter condition field, click the Add button, and then click the Apply filter button. Figure 16 shows an example of the filtered view.

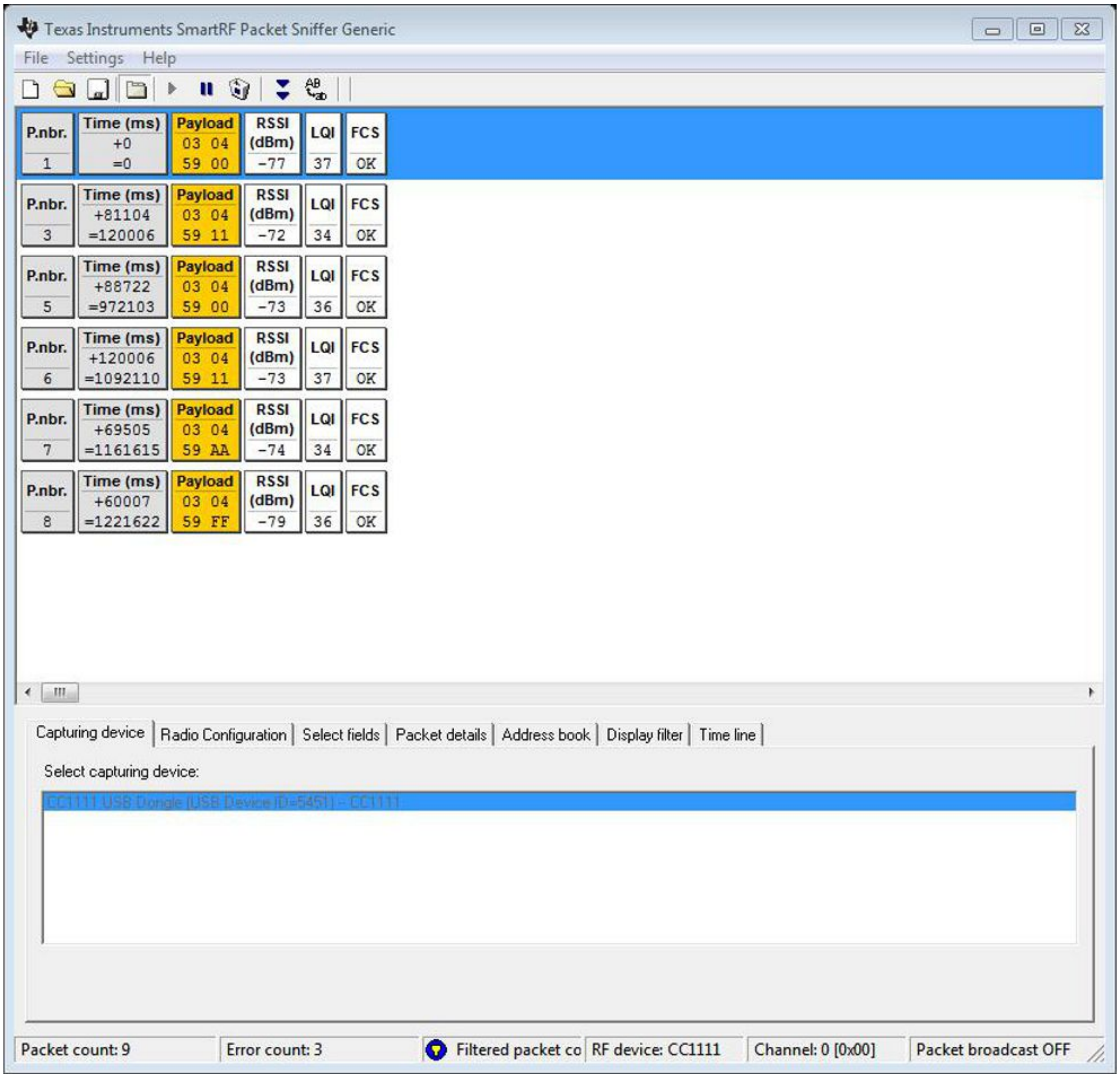

Figure 16. Packet Sniffer Software, Filtered Recording

7. To export the captured, filtered packets, click the "Save the current session" button on the toolbar (appears as a floppy disk), or pause the packet capture and click File → Save data… from the file context menu; either of these choices prompts to save the displayed data as a packet sniffer data (.psd) file.
8. Convert the .psd file to readable hex values with HexEdit software (http://www.hexedit.com/). A different hex editor can perform this function as well; however, the authors of this document have not verified any other options.
9. Open the .psd file in the HexEdit software. Click on Tools → Options. In the HexEdit Options window, click on Document → Display and change the Columns value to "2066". Click Edit → Select All and Edit → Copy As Hex Text. Open a text editor program (for example, Notepad), paste the hex text, and save the text file. This text file can then be imported into Microsoft Excel® spreadsheet software for further analysis. For more information on the sniffer data packet format, click Help → User Manual on the packet sniffer software.

7 Test Setup

7.1 Overview

The Low-Power PIR Motion Detector With Sub-1GHz Wireless Connectivity Enabling 10-Year Coin Cell Battery Life reference design has been characterized to support all of the critical specifications for this sub-system. The following sections describe the test setups for these measurements including the equipment used and the test conditions unless otherwise noted.

7.2 Power Consumption

The power consumption measurements for this reference design were critical in balancing battery lifetime with sensor bias current and motion sensitivity. An initial prototype was built that allowed measurement of the different current paths in the design as a preliminary analysis. The results from that prototype are shown in Section 8.1. Measurements of supply current were then performed on the reference design hardware, which confirmed the prototype measurements. Further characterization was done on the reference design hardware over the voltage range of the design. The test setup for the supply current measurements is illustrated in Figure 17.

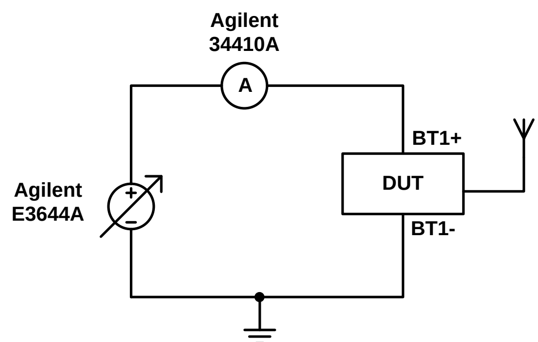

Figure 17. Test Circuit Used for Measuring Supply Current

To compute the battery life, the radio transmission intervals also need to be characterized as these intervals have brief periods of high peak currents before settling to the low microamp current levels measured using the setup above. The measurement of the radio transmission interval involves using a current probe that interfaces to an oscilloscope, which can then be used to trigger on the high current events. Data from this interval is then exported to Microsoft Excel where analysis of the data can be performed. This setup is illustrated in Figure 18.

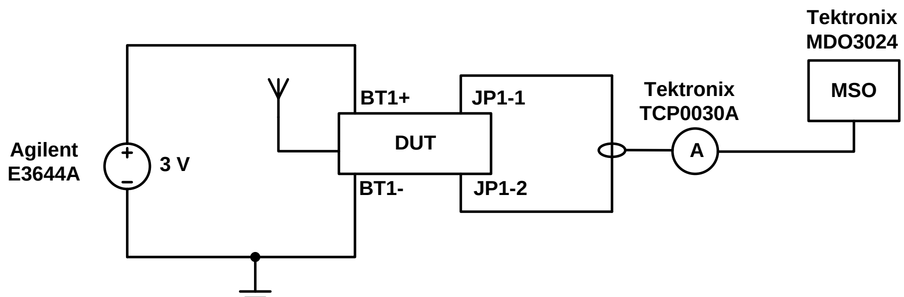

Figure 18. Test Circuit Used for Measuring Supply Current During Radio Transmission Intervals

7.3 Functional

The following subsections describe the tests for functionality under various environmental conditions. These tests generally verify the limits of operation for the subsystem.

7.3.1 Temperature and Humidity Range

This TI Design was stressed under temperature and humidity bias to ensure the design operates and does not produce false triggers under extremes of the targeted environment. The typical extended building environment temperature range is assumed to be 0°C to 50°C while additional testing was performed to test the limits of the design down to –30°C and up to 60°C. Similarly, the typical humidity range for a building environment is assumed to be 20% to 70%.

The chamber used for the temperature and humidity stress was the CSZ ZH322-H/AC Temperature/Humidity Chamber and a Vaisala HMP235 Humidity Probe to monitor humidity. A Watlow F-4 Controller was used to automate the testing. The reference design PCB was placed in the chamber with a new Energizer CR2032 lithium-ion coin cell battery installed. The CC1111 USB dongle was placed near the TI Design hardware inside the chamber and connected to a laptop outside of the chamber with a USB cable to monitor for false triggers during the test. Figure 19 shows a picture of the setup.

Figure 19. Wireless PIR Motion Detector Temperature and Humidity Test Setup

To prevent false detection due to rapid changes in ambient temperature and subsequent sensor settling, the temperature was slowly ramped during the test as would be expected in a typical operating environment. The test was started with a 10-minute soak at 25°C followed by a 1°C per minute ramp up to 50°C with a 5-minute soak, followed by a 5°C per minute ramp to 60°C, and back down to 50°C with a 5-minute soak at 50°C, followed by a 1°C per minute ramp down to 0°C with a 5-minute soak. At 0°C, a similar 5°C per minute ramp was applied down to –30°C and back up to 0°C with a 5-minute soak at 0°C, followed by a 1°C per minute ramp back up to 25°C.

Because of the physical construction of the chamber and its use of fans for air flow within the chamber, false triggers were observed during the temperature ramping periods. During the soaking periods, false triggering subsided over the entire temperature range tested, which proves the functionality of the design over the temperature extremes. This observation is common for PIR-based motion detectors and for this reason are generally not recommended for installation near ventilation. The only known way to prevent the false triggering during this test is to cover the sensor so it could not be affected by thermal gradients due to forced air flow and reflections off the walls of the chamber; however, this was not done as part of this measurement.

To prevent false detection due to rapid changes in humidity, the humidity was slowly ramped during the test as would be expected in a typical operating environment. The test consisted of applying a 1% per minute ramp from 20% to 70% and then back down to 20% with a 30-minute initial soak. The temperature was held at 45°C to prevent condensation; however, condensation was observed at 68% and higher humidity points.

The only anomaly observed during this test was at the point where condensation formed on the PCB, which produced false triggering. As the humidity dropped to a point where the PCB dried, the false triggering stopped and was not observed for the remainder of the test.

7.3.2 Motion Sensitivity

The motion sensitivity range was measured by connecting a dual pulse stretcher design built on a generic prototyping PCB with LED outputs on each channel for visual indication. The inputs to the pulse stretcher are connected to the window comparator output test points of the reference design. Using this method, the PIR sensor was allowed to remain stationary at a fixed location while the LED's indicate when motion is being detected. The pulse stretcher was powered using its own coin cell battery so that it does not interfere with or modify the operation of the PIR sensor being tested. The farthest distance at which reliable detection of motion was indicated was then measured and reported as the motion sensitivity. Pictures of this setup are shown in Figure 20.

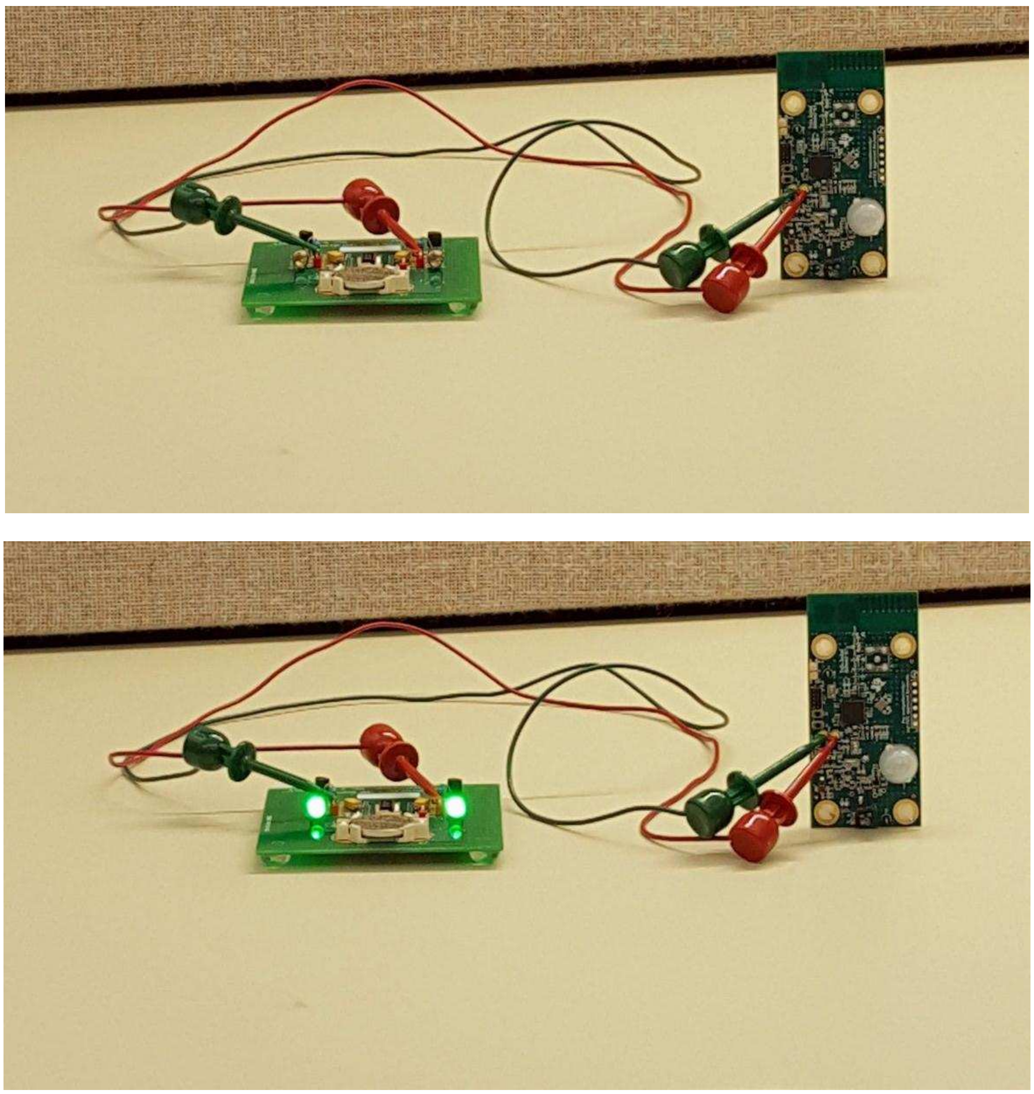

Figure 20. Motion Sensitivity Test Setup
(Top: No Motion; Bottom: Motion Detected)

7.3.3 Wireless RF Range

The range of the Wireless Sub-1GHz RF was measured using the CC1111 USB dongle described in Section 6.2.2. For this test, the PIR PCB remained at a stationary location as a laptop with the CC1111 USB dongle attached and listening was moved away from the PIR PCB. While the CC1111 was on the move, the PIR design was being reset at regular short intervals to make sure there were radio packets constantly being transmitted. The distance at which packets were no longer received was then measured.

Different orientations of the PCB and the CC1111 USB dongle with respect to one another were used during the test. No discernable change in the Wireless RF range was observed.

7.3.4 RF Immunity

The immunity of this TI Design with respect to radiated RF disturbances was measured according to IEC61000-4-3 with an extended low frequency range. The IEC standard is specified for a frequency range of 80 MHz to 1 GHz; however, this testing was extended down to 10 kHz to look for susceptibility in the design for disturbances closer to the pass band of the circuit.

The setup consisted of connecting the pulse stretcher board used in Section 7.3.2 to the window comparator outputs and monitoring the LEDs for activity with a camera inside the anechoic chamber. Additionally, a field strength probe was placed near the board under test for control and monitoring of the RF field strength level being tested. This test setup is shown in Figure 21.

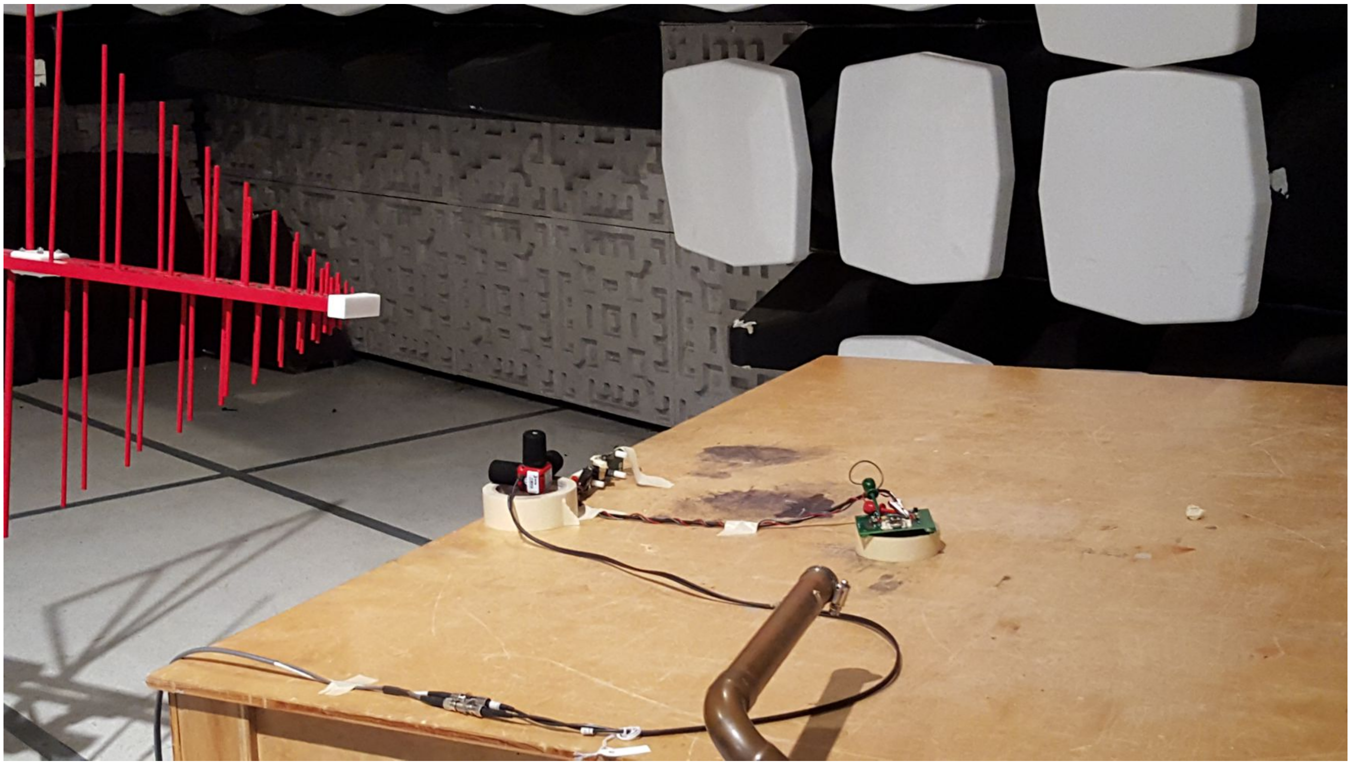

Figure 21. RF Immunity Test Setup

The biconical antenna shown in Figure 21 was used for the frequency range from 30 MHz to 1 GHz in both the horizontal and vertical orientation (vertical orientation shown). For frequencies lower than 30 MHz, it was necessary to use a rod antenna in a single orientation.

8 Test Data

NOTE: Unless otherwise noted, the test data in the following sections were measured with the system at room temperature. All of the measurements in this section were measured with calibrated lab equipment.

8.1 Power Characterization

The supply current for the different circuit paths in this design was measured using an initial prototype design. This information was used early in the design process to balance the battery lifetime with motion sensitivity specifications and the sensor bias. This data was also compared to measurements made on the reference design hardware to make sure there was a good correlation between initial results and final results. Additionally, the reference design hardware was measured versus supply voltage to look at the supply current variation with respect to that variable. The supply current data is shown in the following tables.

Table 2. Low-Power PIR Motion Detector Motion Sensitivity Results

CIRCUIT PATH	SUPPLY CURRENT (IDLE)	
	NOMINAL	MEASURED
Sensor	600 nA	594 nA
Comparators ×2	150 nA	150 nA
Divider	50 nA	50 nA
Opamp1	374 nA	360 nA
Opamp2	409 nA	380 nA
CC1310	100 nA	120 nA
Total	**1.683 µA**	**1.654 µA**

Table 3. Low-Power PIR Motion Detector Motion Sensitivity Results

V_{CC}	SUPPLY CURRENT		
	SHUTDOWN	ACTIVE	DELTA
3.8 V	1.75 µA	2.46 µA	0.71 µA
3.6 V	1.73 µA	2.45 µA	0.72 µA
3.3 V	1.69 µA	2.36 µA	0.67 µA
3.0 V	1.65 µA	2.30 µA	0.65 µA
2.7 V	1.64 µA	2.28 µA	0.64 µA
2.4 V	1.60 µA	2.22 µA	0.62 µA
2.2 V	1.59 µA	N/A	N/A

As can be seen, there is a good correlation between the reference design hardware, the initial prototype measurements, and nominal calculated supply current values. Another observation from Table 3 is that there is a slight positive dependence of supply current on supply voltage, which is expected. However, this also suggests that battery life calculations based on average values will be conservative because the supply current decreases as the battery ages.

The two modes shown in Table 3 relate to the modes described in Figure 9. The Delta column is used to determine the supply current increase between these two modes as this is the value that will be used in the battery life calculations. The highlighted row in Table 3 was included for informational purposes only. At this voltage, the sensor becomes too noisy and starts to generate false triggers. The current in shutdown mode was only measured by programming the user mode to keep the MCU in shutdown and ignore interrupts, which is also why there is no data reported for the Active mode at this supply voltage level.

The values to be used in the battery life calculations from Table 3 are the average current over the range of battery voltages from 3.3 V to 2.4 V. For Shutdown mode, the average current is *1.65 μA* while the average Delta current between Shutdown and Active mode is *0.645 μA*.

The final part of the power characterization was to measure the high current interval during radio transmissions when changing modes. The oscilloscope picture of this event is shown in Figure 22 and Figure 23.

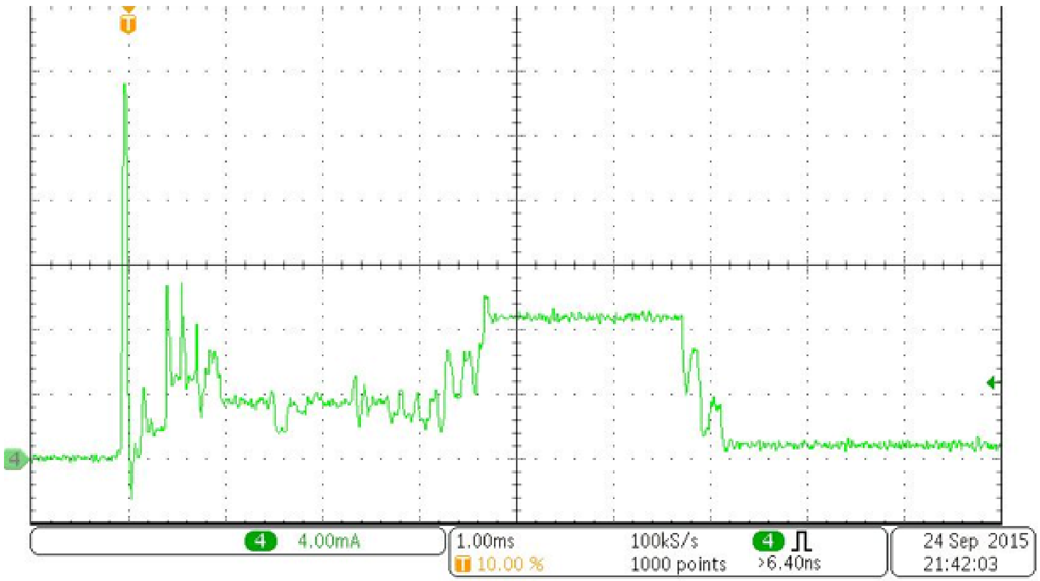

Figure 22. Radio Transmission Event Supply Current (Zoomed in)

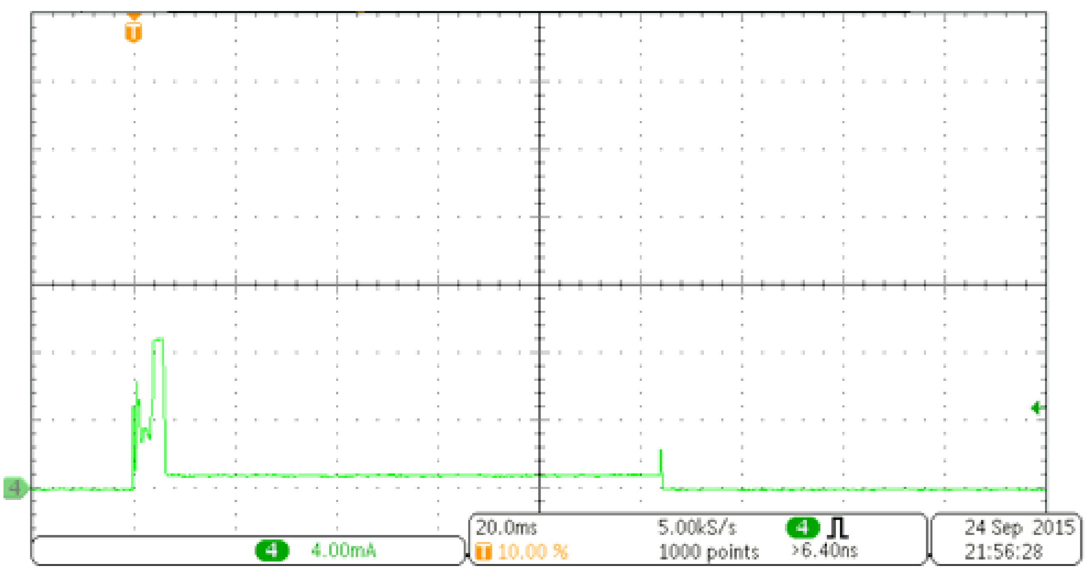

Figure 23. Radio Transmission Event Supply Current (Full Picture)

The results for the average current calculation during the radio transmission interval from Excel is 1.12 mA over a total duration of 104.1 ms.

The data values highlighted in this section are used in the following section to calculate the expected battery life for different expected use conditions.

8.2 Battery Life Calculations

The computation of battery life for this reference design is complicated by the myriad of different applications and use conditions possible for this type of sensor node. The approach taken here computes the average between two different expected likely use conditions and the worst case use condition. These use conditions are described as follows:

- *Case 1: Worst case*: 10 motion events per hour for every hour for the life of the battery. Each of these motion events is a walk through event meaning that an interrupt is generated by a body moving through the field of view once, allowing the active timer to expire and re-enter Shutdown mode before the next event occurs.
- *Case 2: Busy room in an office environment case*: 14 hours in Shutdown, 10 hours with constant motion such that the active timer does not expire once activated.
- *Case 3: Room with intermittent motion during business hours case*: 14 hours in Shutdown, 10 hours with 10 motion events per hour every hour. Similar to Case 1, each of these events is a walk through event.

Another available knob in the optimization of battery life for this reference design is the active timer value. The default value in firmware is 1 minute. Since this value can be modified, the battery life for Case 1 and Case 3 are recalculated using a value of 30 seconds to show the expected improvement.

The equations for the expected battery life for the three cases in consideration are as follows.

General lifetime equation:

$$\text{Lifetime} = \frac{\text{Battery Capacity}}{\text{Shutdown Current + Event Current}} \times \frac{1}{8760\,\text{hr / yr}} \times \text{Derating Factor} \tag{13}$$

where

- $\text{Event Current} = \left[(\text{Delta Current} \times \text{Active Mode Duty Cycle}) + (\text{Radio Transmission Current} \times \text{Duty Cycle})\right] \times \text{Number of Events}$

Case 1

$$\text{Lifetime} = \frac{240\ \text{mAH}}{\left\{1.65\ \mu\text{A} + \left[\left((645\ \text{nA} \times 60\,\text{s / event}) + (1.12\ \text{mA} \times 104.1\ \text{ms / event} \times 2)\right) \times \frac{10\ \text{events / hr}}{3600\ \text{s / hr}}\right]\right\}} \times \frac{1}{8760\ \text{hr / yr}} \times 0.85 = 9.68\ \text{years}$$

Case 2

$$\text{Lifetime} = \frac{240\ \text{mAH}}{1.65\ \mu\text{A} + 645\ \text{nA}\left(\frac{10\,\text{hours}}{24\,\text{hours}}\right) + \left[(1.12\ \text{mA} \times 104.1\ \text{ms / event}) \times \frac{2\ \text{events / day}}{(3600\ \text{s / hr})(24\ \text{hr / day})}\right]} \times \frac{1}{8760\ \text{hr / yr}} \times 0.85 = 12.12\ \text{years}$$

Case 3

$$\text{Lifetime} = \frac{240\,\text{mAH}}{\left\{1.65\ \mu\text{A} + \left[\left((645\ \text{nA} \times 60\ \text{s / event}) + (1.12\ \text{mA} \times 104.1\ \text{ms / event} \times 2)\right) \times \frac{10\ \text{events / hr}}{3600\ \text{s / hr}} \times \frac{10\ \text{hours}}{24\ \text{hours}}\right]\right\}} \times \frac{1}{8760\ \text{hr / yr}} \times 0.85 = 11.85\ \text{years}$$

The derating factor in these equations accounts for self aging of the battery. Based on these equations, the average expected battery lifetime for this reference design with the active timer set to 1 minute is *11.22 years*. Re-calculating Case 1 and Case 3 with an active timer set to 30 seconds is 9.9 years and 11.99 years, respectively. The average expected battery life with an active timer value of 30 seconds is therefore *11.34 years*. By inspection, decreasing the active timer to 17 seconds or less will yield a worst case estimated battery lifetime of at least 10 years.

8.3 Functional

8.3.1 Motion Sensitivity

The motion sensitivity was measured for multiple sensors with different bias conditions and two different gain settings. Table 4 summarize these measurement results.

Table 4. Low-Power PIR Motion Detector Motion Sensitivity Results

SENSOR	SUPPLY CURRENT (IDLE)	V_{OUT} (DC)	MAX. DISTANCE (Av = 90 dB)	MAX. DISTANCE (Av = 70 dB)
RS = 2.2 MΩ, RD = 1 MΩ				
IRS-B210ST01	365 nA	0.78 V	20 ft	6 ft
IRS-B340ST02	355 nA	0.764 V	25 ft	8 ft
IRA-E700ST0	500 nA	1.093 V	12 ft	4.5 ft
IRA-E712ST3	555 nA	1.204 V	13 ft	5 ft
RS = 1.3 MΩ, RD = 620 KΩ				
IRS-B210ST01	594 nA	0.77 V	> 30 ft	6.5 ft
IRS-B340ST02	572 nA	0.744 V	27 ft	8 ft
IRA-E700ST0	838 nA	1.085 V	15 ft	5 ft
IRA-E712ST3	920 nA	1.178 V	17 ft	7.5 ft

The highlighted cell in Table 4 illustrates the motion sensitivity of the circuit configuration implemented in this TI Design.

8.3.2 Wireless RF Range

The wireless RF range was measured to be 220 meters in a typical office environment with partial line of sight. The measured signal strength at this distance was less than –100 dBm as measured by the CC1111 packet sniffer dongle.

While this distance is outstanding considering the small footprint of the PCB antenna, there are ways to increase this distance even further. Use of a whip antenna with gain instead of the passive PCB antenna could offer improvements in the wireless RF range. Another option would be to increase the transmit power of the CC1310 to its maximum level at the expense of increased supply current during the radio transmission intervals.

8.3.3 RF Immunity

The RF immunity of this design was measured to be 30 V/m over the entire 10-kHz to 1-GHz frequency range. Immunity at field strengths higher than this were not tested due to equipment limitations in the frequency range around 30 MHz. This level also corresponds to Class 3 in the IEC61000-4-3 standard.

The only anomaly observed during this test was at the singular frequency step of 728.5 MHz, where the passing immunity level dropped to 29.8 V/m in the horizontal antenna orientation. This drop was due to the wiring connection between the PIR PCB and the pulse stretcher board used for monitoring.

8.3.4 Vibration

Vibration was not tested on this reference design in any official capacity. Part of the reasoning for this is that finding vibration specifications on commercially available PIR motion detectors is difficult to find. Rudimentary vibration testing was performed in the lab by beating on the desk on which the PIR was also resting and looking for false trigger events at the output of the window comparator. Based on this test, no false triggers were observed as long as the PCB did not physically move. While crude, this test does show that there is nothing systematic in the design itself that would cause false triggers in a normal application aside from the sensor construction itself.

A more informative test would include control over vibration frequency and amplitude with both of these being varied. The results of such a test would illustrate potential harmonic sensitivities to vibration. PCB orientation could also be varied as part of this test for a complete picture of the sensitivity to vibration for a given design in different installations. Because such an elaborate test would yield different results based on the physical enclosure that would finally house the PCB design, it was determined that this was beyond the scope of this reference design.

All PIR-based motion sensors are sensitive to vibration in some capacity due to the physical construction of the sensor as well as the way it naturally operates. Because the PIR sensor is built using thermopiles, these elements have a crystal structure, which exhibits a piezo-electric effect if the amplitude and frequency of vibration is such that the thermopiles themselves vibrate. A more prevalent effect is due to the entire sensor itself moving. Because a Fresnel lens enlarges the effective field of view of the sensor at substantial distances away from the sensor by focusing IR energy onto the small area of the sensor elements, any small movement of the sensor will result in large movements in the field of view. Due to background IR energy, the sensor output will not be able to distinguish between changes in IR energy due to motion with a static background or the background itself changing rapidly due to movements of the field of view. In other words, the detection of motion is relative. If the sensor is assumed to be perfectly static, motion detected will be relative to the sensor, however, motion will also be detected if the background is static but the sensor is moving. In both cases, the output is valid because there is motion, but the task of narrowing the output to what is desired falls upon the installation and enclosure design.

9 Design Files

9.1 Schematics

To download the schematics, see the design files at TIDA-00489.

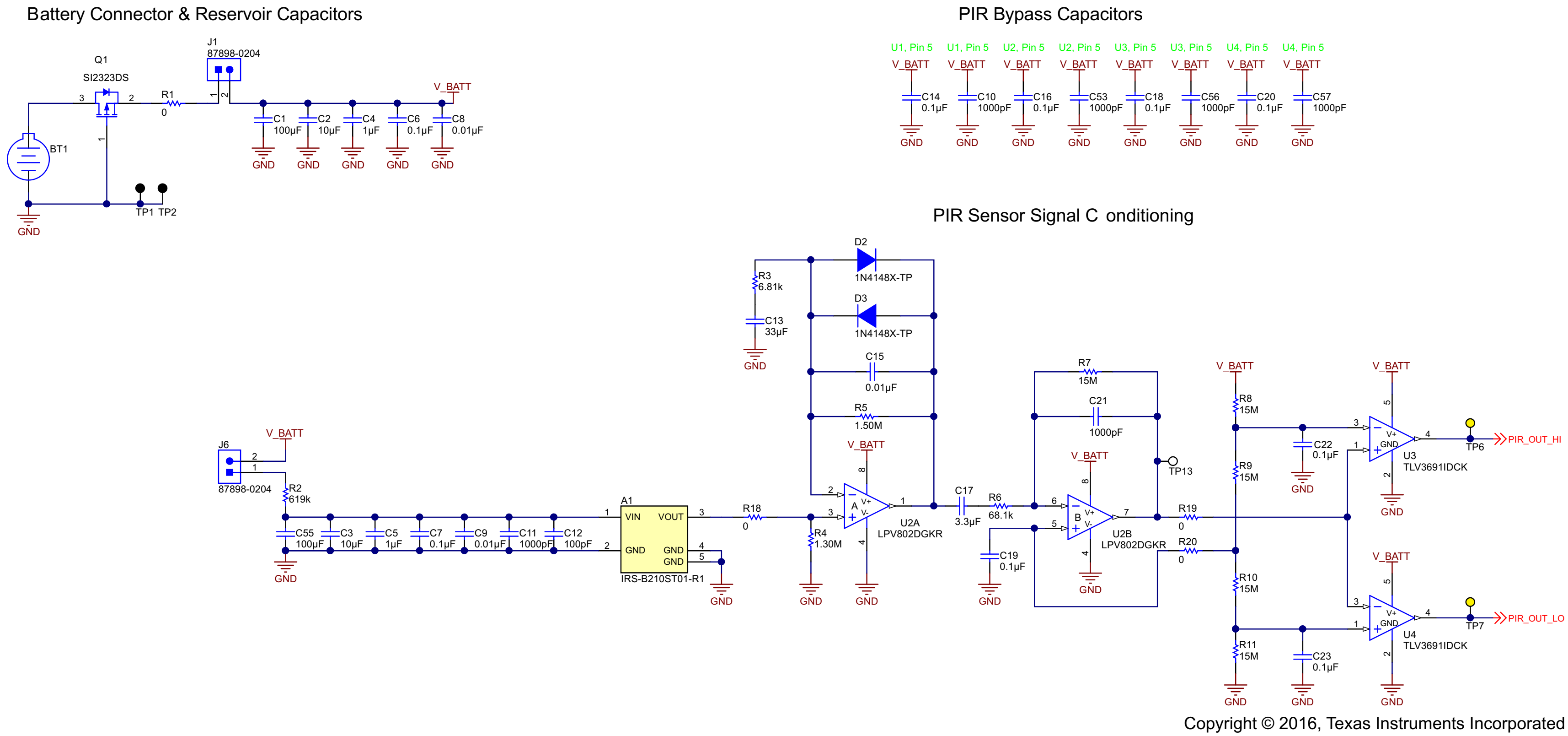

Figure 24. Power and PIR Sensor Schematic

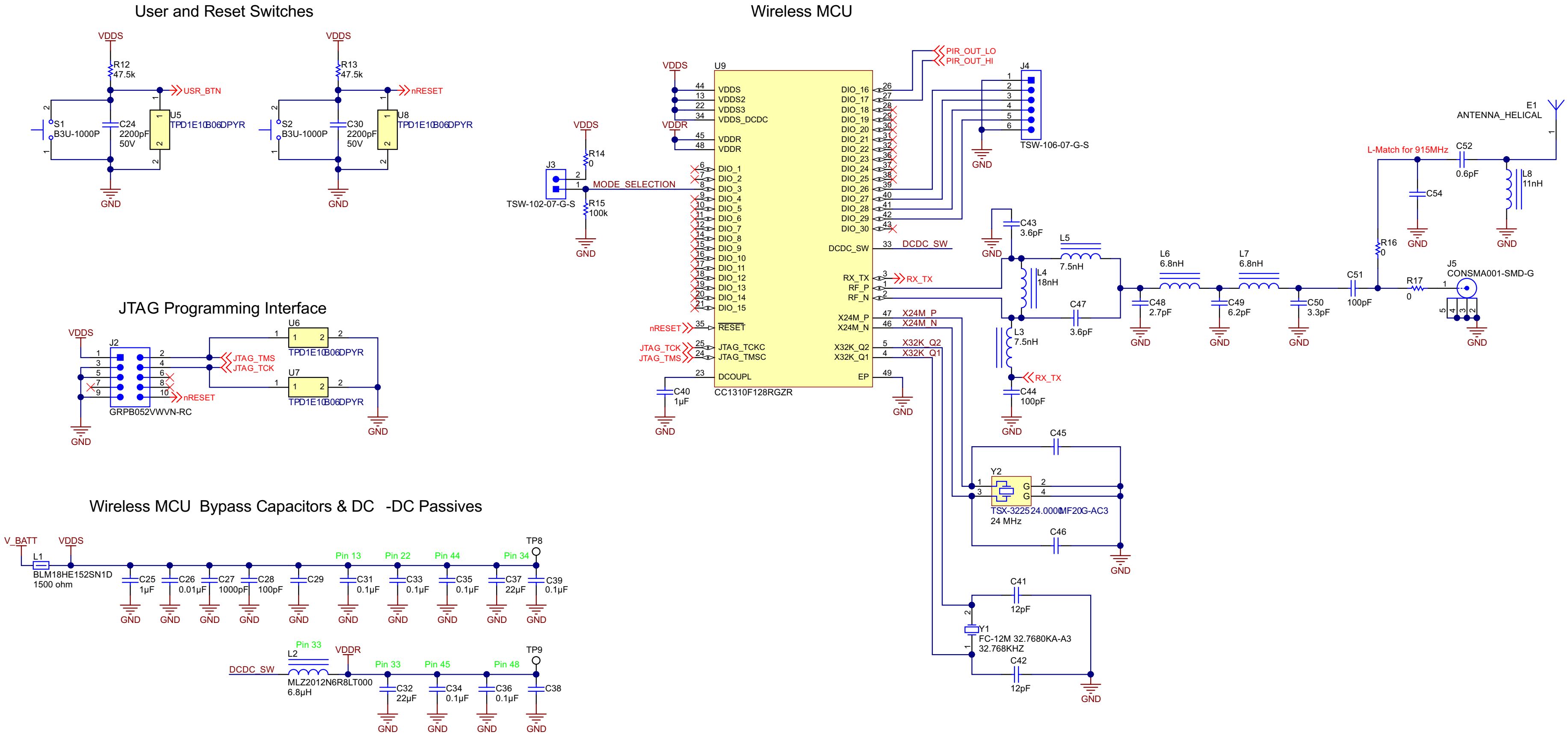

Figure 25. Wireless MCU Schematic

9.2 Bill of Materials

To download the bill of materials (BOM), see the design files at TIDA-00489.

Table 5. Low-Power PIR Motion Detector With Sub-1GHz Wireless Connectivity Enabling 10-Year Coin Cell Battery Life BOM

ITEM	DESIGNATOR	QTY	VALUE	PARTNUMBER	MANUFACTURER	DESCRIPTION	PACKAGE REFERENCE
1	!PCB1	1		ISE4042	Any	Printed Circuit Board	
2	A1	1	3.6mVp-p	IRS-B210ST01-R1	MuRata	Pyroelectric Infrared Sensors for Reflow Soldering, 3.6mVp-p, SMD	4.7x4.7mm
3	BT1	1		BS-7	Memory Protection Devices	Battery Holder, CR2032, Retainer clip, TH	CR2032 holder
4	C1, C55	2	100uF	C3216X5R1A107M160AC	TDK	CAP, CERM, 100 µF, 10 V, +/- 20%, X5R, 1206_190	1206_190
5	C2	1	10uF	C1608X5R0J106M	TDK	CAP, CERM, 10 µF, 6.3 V, +/- 20%, X5R, 0603	0603
6	C3	1	10uF	GRM155R60J106ME44D	MuRata	CAP, CERM, 10 µF, 6.3 V, +/- 20%, X5R, 0402	0402
7	C4, C25	2	1uF	C1608X7R1C105K	TDK	CAP, CERM, 1 µF, 16 V, +/- 10%, X7R, 0603	0603
8	C5	1	1uF	C1005X5R1A105K050BB	TDK	CAP, CERM, 1 µF, 10 V, +/- 10%, X5R, 0402	0402
9	C6, C7	2	0.1uF	C1005X7R1H104K050BB	TDK	CAP, CERM, 0.1 µF, 50 V, +/- 10%, X7R, 0402	0402
10	C8, C9, C26	3	0.01uF	C1005X7R1C103K	TDK	CAP, CERM, 0.01 µF, 16 V, +/- 10%, X7R, 0402	0402
11	C10, C11, C27, C53, C56, C57	6	1000pF	C1005X7R1H102K	TDK	CAP, CERM, 1000 pF, 50 V, +/- 10%, X7R, 0402	0402
12	C12, C28	2	100pF	C0402C101J3GACTU	Kemet	CAP, CERM, 100 pF, 25 V, +/- 5%, C0G/NP0, 0402	0402
13	C13	1	33uF	C2012X5R1A336M125AC	TDK	CAP, CERM, 33 µF, 10 V, +/- 20%, X5R, 0805	0805
14	C14, C16, C18, C19, C20, C22, C23	7	0.1uF	C1005X7R1H104K	TDK	CAP, CERM, 0.1 µF, 50 V, +/- 10%, X7R, 0402	0402
15	C15	1	0.01uF	C1005X7R1E103K	TDK	CAP, CERM, 0.01 µF, 25 V, +/- 10%, X7R, 0402	0402
16	C17	1	3.3uF	C1005X5R1A335K050BC	TDK	CAP, CERM, 3.3 µF, 10 V, +/- 10%, X5R, 0402	0402
17	C21	1	1000pF	C1005C0G1E102J	TDK	CAP, CERM, 1000 pF, 25 V, +/- 5%, C0G/NP0, 0402	0402
18	C24, C30	2	2200pF	C1005X7R1H222K	TDK	CAP, CERM, 2200 pF, 50 V, +/- 10%, X7R, 0402	0402
19	C31, C33, C34, C35, C36, C39	6	0.1uF	GRM155R70J104KA01D	MuRata	CAP, CERM, 0.1 µF, 6.3 V, +/- 10%, X7R, 0402	0402

Table 5. Low-Power PIR Motion Detector With Sub-1GHz Wireless Connectivity Enabling 10-Year Coin Cell Battery Life BOM (continued)

ITEM	DESIGNATOR	QTY	VALUE	PARTNUMBER	MANUFACTURER	DESCRIPTION	PACKAGE REFERENCE
20	C32, C37	2	22uF	C1608X5R0J226M080AC	TDK	CAP, CERM, 22 µF, 6.3 V, +/- 20%, X5R, 0603	0603
21	C40	1	1uF	GRM188R70J105KA01D	MuRata	CAP, CERM, 1 µF, 6.3 V, +/- 10%, X7R, 0603	0603
22	C41, C42	2	12pF	GRM1555C1E120JA01D	MuRata	CAP, CERM, 12 pF, 25 V, +/- 5%, C0G/NP0, 0402	0402
23	C43, C47	2	3.6pF	GRM1555C1H3R6CA01D	MuRata	CAP, CERM, 3.6 pF, 50 V, +/- 5%, C0G/NP0, 0402	0402
24	C44, C51	2	100pF	GRM1555C1H101JA01D	MuRata	CAP, CERM, 100 pF, 50 V, +/- 5%, C0G/NP0, 0402	0402
25	C48	1	2.7pF	GRM1555C1H2R7CA01D	MuRata	CAP, CERM, 2.7 pF, 50 V, +/- 5%, C0G/NP0, 0402	0402
26	C49	1	6.2pF	GRM1555C1H6R2CA01D	MuRata	CAP, CERM, 6.2 pF, 50 V, +/- 5%, C0G/NP0, 0402	0402
27	C50	1	3.3pF	GRM1555C1H3R3CA01D	MuRata	CAP, CERM, 3.3 pF, 50 V, +/- 5%, C0G/NP0, 0402	0402
28	C52	1	0.6pF	GJM1555C1HR60BB01D	Murata	CAP, CERM, 0.6pF, 50V, NP0/C0G, +-0.1pF, 0402	0402
29	D2, D3	2	75V	1N4148X-TP	Micro Commercial Components	Diode, Switching, 75 V, 0.3 A, SOD-523	SOD-523
30	E1	1		ANTENNA_HELICAL	N/A	PCB Antenna. There is nothing to buy or mount.	Antenna
31	H1, H4, H6, H8	4		NY PMS 440 0025 PH	B&F Fastener Supply	Machine Screw, Round, #4-40 x 1/4, Nylon, Philips panhead	Screw
32	H2, H3, H5, H7	4		1902C	Keystone	Standoff, Hex, 0.5"L #4-40 Nylon	Standoff
33	H9	1		IML-0669	MuRata	Lens, Ceiling Mount, TH	D12xH8.508mm
34	J1, J6	2		87898-0204	Molex	Header, 2.54 mm, 2x1, Gold, R/A, SMT	Header, 2.54 mm, 2x1, R/A, SMT
35	J2	1		GRPB052VWVN-RC	Sullins Connector Solutions	Header, 50mil, 5x2, Gold, TH	Header, 5x2, 50mil
36	J3	1		TSW-102-07-G-S	Samtec	Header, 100mil, 2x1, Gold, TH	2x1 Header
37	L1	1	1500 ohm	BLM18HE152SN1D	MuRata	Ferrite Bead, 1500 ohm @ 100 MHz, 0.5 A, 0603	0603
38	L2	1	6.8uH	MLZ2012N6R8LT000	TDK	Inductor, Multilayer, Ferrite, 6.8 µH, 0.11 A, 0.25 ohm, SMD	0805
39	L3, L5	2	7.5nH	LQW15AN7N5G00D	MuRata	Inductor, Wirewound, 7.5 nH, 0.57 A, 0.13 ohm, SMD	1x.5x.5mm
40	L4	1	18nH	LQW15AN18NJ00D	MuRata	Inductor, Wirewound, 18 nH, 0.37 A, 0.27 ohm, SMD	1x.5x.5mm

Table 5. Low-Power PIR Motion Detector With Sub-1GHz Wireless Connectivity Enabling 10-Year Coin Cell Battery Life BOM (continued)

ITEM	DESIGNATOR	QTY	VALUE	PARTNUMBER	MANUFACTURER	DESCRIPTION	PACKAGE REFERENCE
41	L6, L7	2	6.8nH	LQW15AN6N8G00D	MuRata	Inductor, Wirewound, 6.8 nH, 0.7 A, 0.09 ohm, SMD	1x.5x.5mm
42	L8	1	11nH	LQW15AN11NG00D	MuRata	Inductor, Wirewound, 11 nH, 0.5 A, 0.14 ohm, SMD	1x.5x.5mm
43	Q1	1	-20V	SI2323DS	Vishay-Siliconix	MOSFET, P-CH, -20 V, -3.7 A, SOT-23	SOT-23
44	R1	1	0	CRCW08050000Z0EA	Vishay-Dale	RES, 0, 5%, 0.125 W, 0805	0805
45	R2	1	619k	CRCW0402619KFKED	Vishay-Dale	RES, 619 k, 1%, 0.063 W, 0402	0402
46	R3	1	6.81k	CRCW04026K81FKED	Vishay-Dale	RES, 6.81 k, 1%, 0.063 W, 0402	0402
47	R4	1	1.30Meg	CRCW04021M30FKED	Vishay-Dale	RES, 1.30 M, 1%, 0.063 W, 0402	0402
48	R5	1	1.50Meg	CRCW04021M50FKED	Vishay-Dale	RES, 1.50 M, 1%, 0.063 W, 0402	0402
49	R6	1	68.1k	CRCW040268K1FKED	Vishay-Dale	RES, 68.1 k, 1%, 0.063 W, 0402	0402
50	R7, R8, R9, R10, R11	5	15Meg	RMCF0805JT15M0	Stackpole Electronics Inc	RES, 15 M, 5%, 0.125 W, AEC-Q200 Grade 0, 0805	0805
51	R12, R13	2	47.5k	CRCW040247K5FKED	Vishay-Dale	RES, 47.5 k, 1%, 0.063 W, 0402	0402
52	R14, R16, R18, R19, R20	5	0	CRCW04020000Z0ED	Vishay-Dale	RES, 0, 5%, 0.063 W, 0402	0402
53	R15	1	100k	CRCW0402100KFKED	Vishay-Dale	RES, 100 k, 1%, 0.063 W, 0402	0402
54	S1, S2	2		B3U-1000P	Omron Electronic Components	SWITCH TACTILE SPST-NO 0.05A 12V	3x1.6x2.5mm
55	SH-J1, SH-J3, SH-J6	3	1x2	969102-0000-DA	3M	Shunt, 100mil, Gold plated, Black	Shunt
56	TP1, TP2	2	Black	5001	Keystone	Test Point, Miniature, Black, TH	Black Miniature Testpoint
57	TP6, TP7	2	Yellow	5004	Keystone	Test Point, Miniature, Yellow, TH	Yellow Miniature Testpoint
58	TP8, TP9, TP13	3	SMT	5015	Keystone	Test Point, Miniature, SMT	Testpoint_Keystone_Miniature
59	U2A, U2B	2		LPV802DGKR	Texas Instruments	350 nA Rail-to-Rail I/O Nanopower Operational Amplifier Family, DGK0008A	DCK0005A
60	U3, U4	2		TLV3691IDCK	Texas Instruments	0.9-V to 6.5-V, Nanopower Comparator, DCK0005A	DCK0005A
61	U5, U6, U7, U8	4		TPD1E10B06DPYR	Texas Instruments	ESD in 0402 Package with 10 pF Capacitance and 6 V Breakdown, 1 Channel, -40 to +125 degC, 2-pin X2SON (DPY), Green (RoHS & no Sb/Br)	DPY0002A
62	U9	1		CC1310F128RGZR	Texas Instruments	Sub-1 GHz and 2.4 GHz Multi-standard RF IC Family, RGZ0048A	RGZ0048A
63	Y1	1		FC-12M 32.7680KA-A3	Epson	Crystal, 32.768kHz, 12.5pF, SMD	Crystal 2.05x.6x1.2mm

Table 5. Low-Power PIR Motion Detector With Sub-1GHz Wireless Connectivity Enabling 10-Year Coin Cell Battery Life BOM (continued)

ITEM	DESIGNATOR	QTY	VALUE	PARTNUMBER	MANUFACTURER	DESCRIPTION	PACKAGE REFERENCE
64	Y2	1		TSX-3225 24.0000MF20G-AC3	Epson	Crystal, 24 MHz, 9 pF, SMD	SMD, 4-Leads, Body 2.65x3.35mm, Height 0.6mm
65	C29	0	22uF	C1608X5R0J226M080AC	TDK	CAP, CERM, 22 µF, 6.3 V, +/- 20%, X5R, 0603	0603
66	C38	0	0.1uF	GRM155R70J104KA01D	MuRata	CAP, CERM, 0.1 µF, 6.3 V, +/- 10%, X7R, 0402	0402
67	C45, C46	0	12pF	GRM1555C1E120JA01D	MuRata	CAP, CERM, 12 pF, 25 V, +/- 5%, C0G/NP0, 0402	0402
68	C54	0	1pF	GRM1555C1H1R0CA01D	MuRata	CAP, CERM, 1 pF, 50 V, +/- 5%, C0G/NP0, 0402	0402
69	FID1, FID2, FID3, FID4, FID5, FID6	0		N/A	N/A	Fiducial mark. There is nothing to buy or mount.	N/A
70	J4	0		TSW-106-07-G-S	Samtec	Header, 100mil, 6x1, Gold, TH	6x1 Header
71	J5	0		CONSMA001-SMD-G	Linx Technologies	Jack, SMA, PCB, Gold, SMT	SMA Jack
72	R17	0	0	CRCW04020000Z0ED	Vishay-Dale	RES, 0, 5%, 0.063 W, 0402	0402

9.3 PCB Layout Recommendations

To ensure high performance, the Low-Power PIR Motion Detector With Sub-1GHz Wireless Connectivity Enabling 10-Year Coin Cell Battery Life TI Design was laid out using a four-layer PCB. The second layer is a solid GND pour, and the third layer is used for power rail routing with GND fills in unused areas. The top and bottom layers are used for general signal routing and also have GND fills in unused areas. For all of the TI products used in this TI Design, adhere to the layout guidelines detailed in their respective datasheets.

Additionally, because of the low-power design and the resulting high-impedance paths present in the design, keep the signal routes in the analog sensor path between the PIR sensor output and the window comparator input as short as possible with adequate GND fill around these signals.

If this design is to be used in an environment where dust or moisture accumulation is possible, be aware that it may be necessary to include a conformal coating to eliminate additional leakage paths due to the operating environment over time.

The antenna on this TI Design is the miniature helical PCB antenna for 868 MHz or 915 MHz. See the application note DN038 (SWRA416) for more details about layout and performance.

9.3.1 Layout Prints

To download the layout prints, see the design files at TIDA-00489.

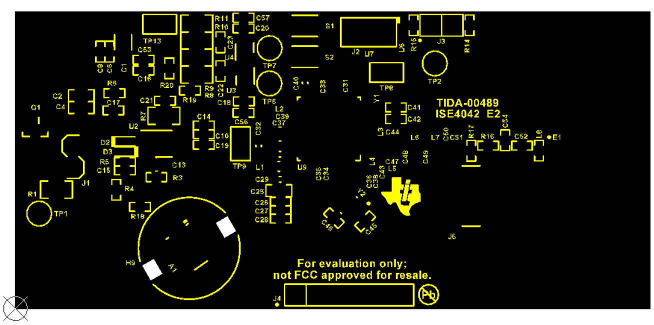

Figure 26. Top Silkscreen

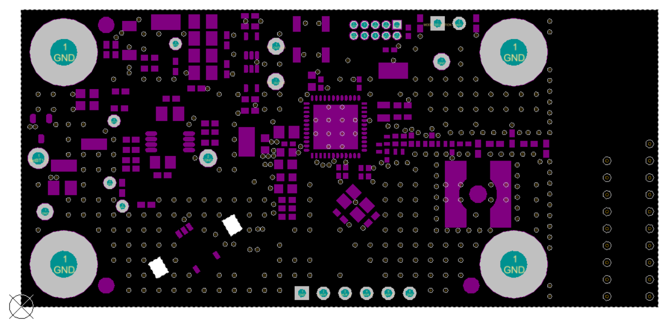

Figure 27. Top Solder Mask

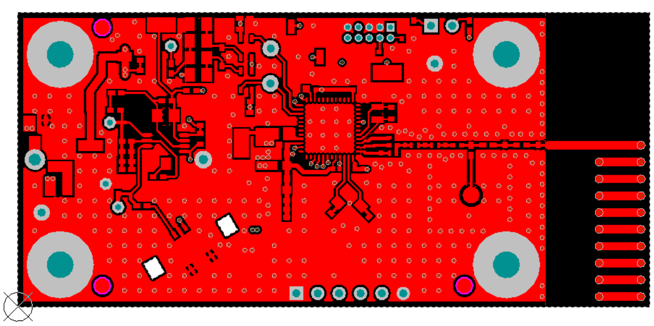

Figure 28. Top Layer

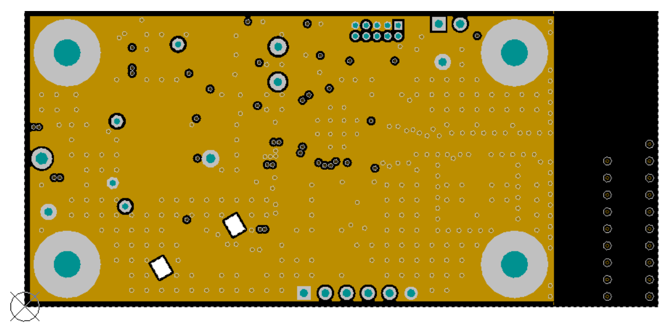

Figure 29. GND Layer

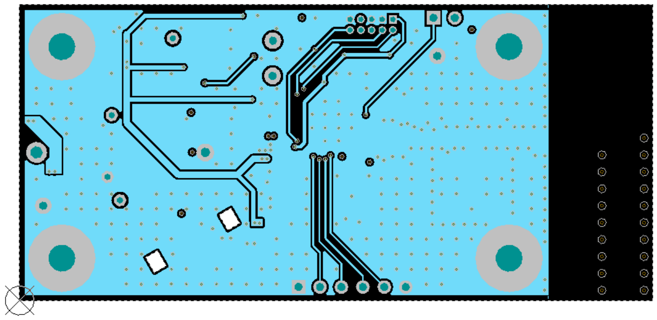

Figure 30. Power Layer

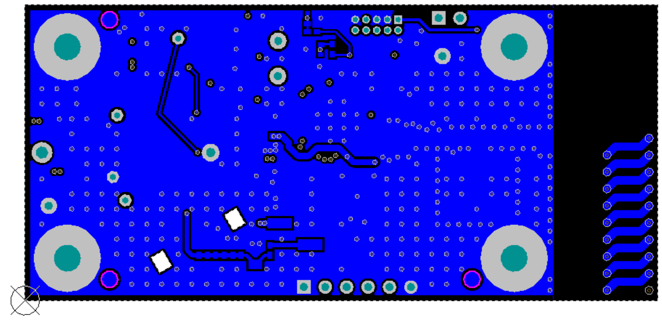

Figure 31. Bottom Layer

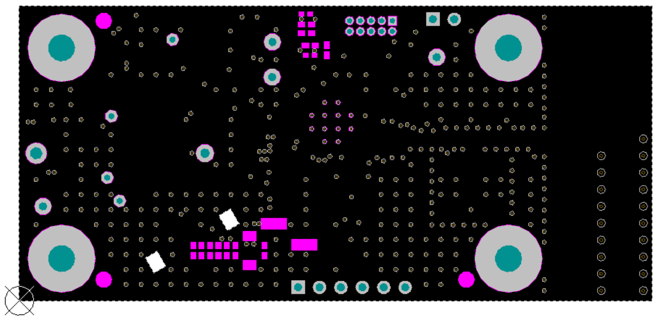

Figure 32. Bottom Solder Mask

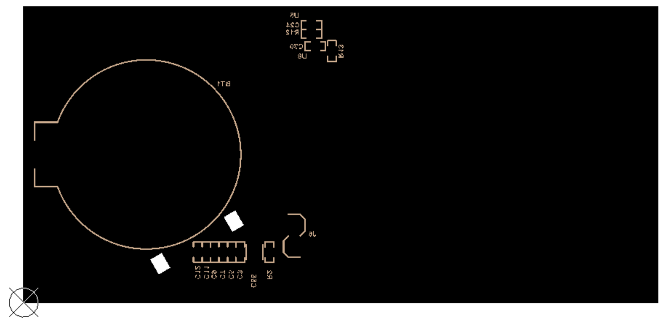

Figure 33. Bottom Silkscreen

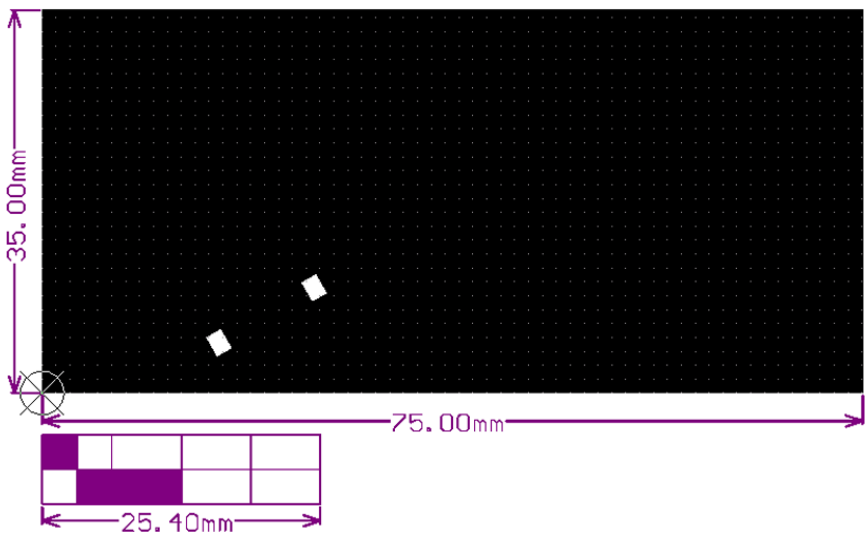

Figure 34. Board Dimensions

9.4 Altium Project

To download the Altium project files, see the design files at TIDA-00489.

9.5 Layout Guidelines

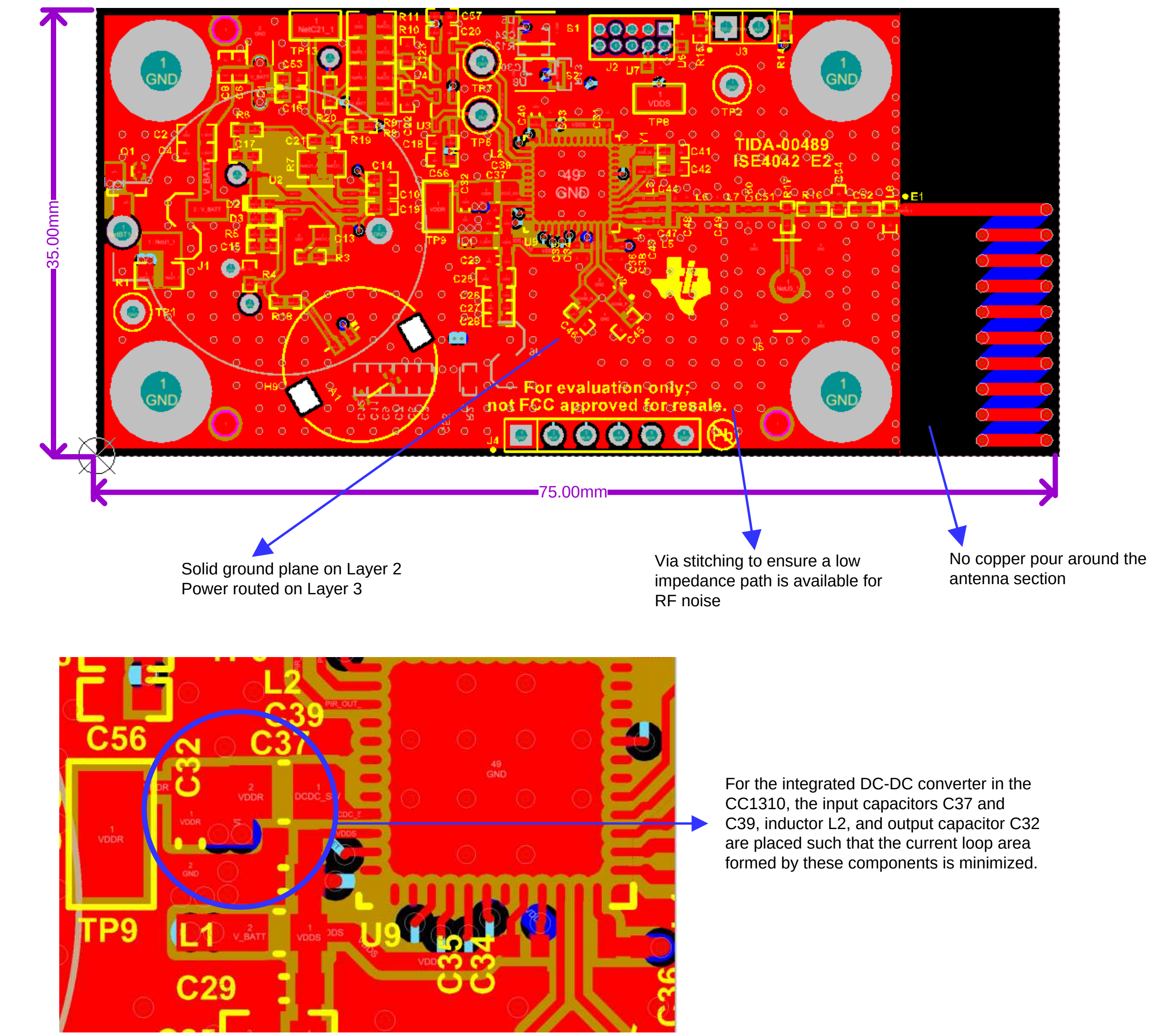

Figure 35. Low-Power PIR Motion Detector Reference Design Layout Guidelines

9.6 Gerber Files

To download the Gerber files, see the design files at TIDA-00489.

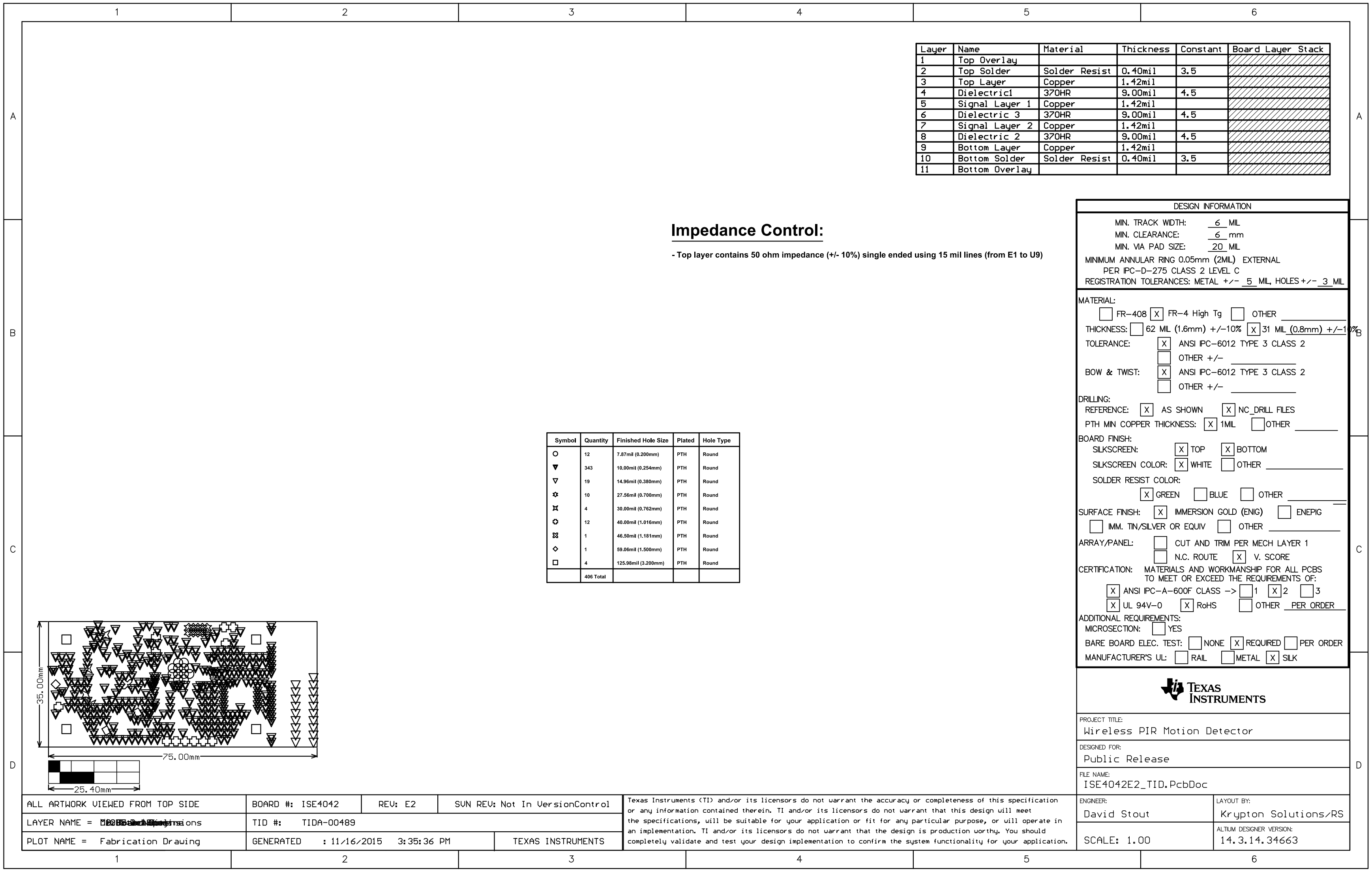

Figure 36. Fabrication Drawing

9.7 Assembly Drawings

To download the assembly drawings, see the design files at TIDA-00489.

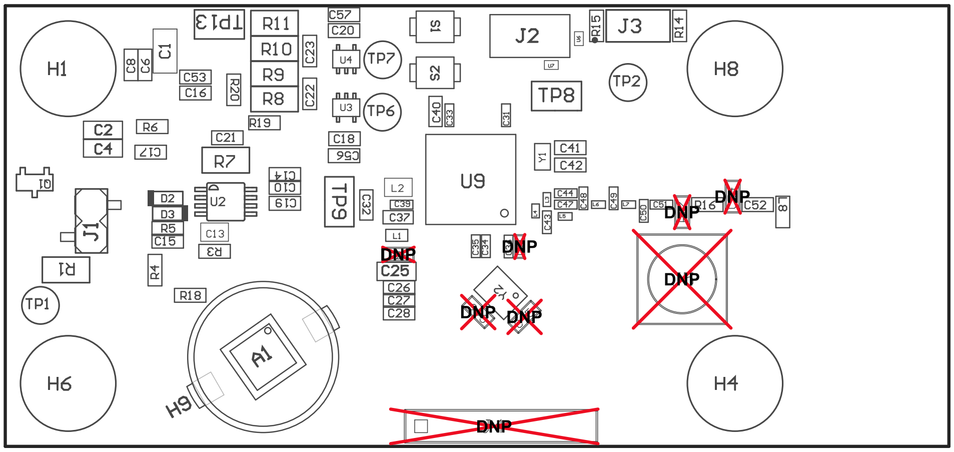

Figure 37. Top Assembly Drawing

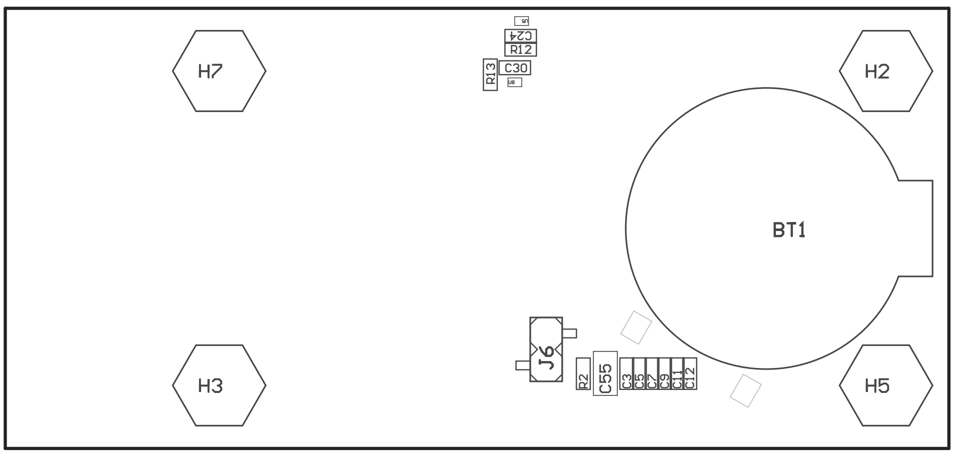

Figure 38. Bottom Assembly Drawing

10 Software Files

To download the software files, see the design files at TIDA-00489.

11 References

1. Texas Instruments, *Reverse Current/Battery Protection Circuits*, Application Report (SLVA139)
2. Texas Instruments, *Coin Cells and Peak Current Draw*, WP001 White Paper (SWRA349)
3. Texas Instruments, *Miniature Helical PCB Antenna for 868 MHz or 915/920 MHz*, DN038 Application Report (SWRA416)
4. Texas Instruments WEBENCH® Design Center (http://www.ti.com/webench)

12 About the Authors

DAVID STOUT is a systems designer at Texas Instruments, where he is responsible for developing reference designs in the industrial segment. David has over 18 years of experience designing Analog, Mixed-Signal, and RF ICs with more than 14 years focused on products for the industrial semiconductor market. David earned his bachelor of science in electrical engineering (BSEE) degree from Louisiana State University, Baton Rouge, Louisiana and a master of science in electrical engineering (MSEE) degree from the University of Texas at Dallas, Richardson, Texas.

CHRISTINA S. LAM is a systems architect at Texas Instruments, where she is responsible for developing firmware for reference design solutions in the industrial segment. Christina has broad experience with applications processors, microcontrollers, and digital-signal processors with specialties in embedded firmware. Christina earned her bachelor of science (BS) in electrical and computer engineering from the University of Texas at Austin.

Revision B History

NOTE: Page numbers for previous revisions may differ from page numbers in the current version.

Changes from A Revision (December 2015) to B Revision **Page**

- Changed LPV521 to LPV802 in Design Resources 1
- Changed the amplified bandpass filter from LPV521 to LPV802 1
- Changed all instances of LPV521 to LPV802 3
- Changed amplified bandpass filter in Figure 1 from LPV521 to LPV802 6
- Changed Ax in Figure 5 from LPV521 to LPV802 13
- Changed Figure 24 to reflect LPV802 35
- Changed Figure 25 to reflect LPV802 36
- Changed Figure 26 to reflect LPV802 41
- Changed Figure 27 to reflect LPV802 41
- Changed Figure 28 to reflect LPV802 41
- Changed Figure 29 to reflect LPV802 41
- Changed Figure 30 to reflect LPV802 41
- Changed Figure 31 to reflect LPV802 41
- Changed Figure 32 to reflect LPV802 42
- Changed Figure 33 to reflect LPV802 42
- Changed Figure 35 to reflect LPV802 43
- Changed Figure 37 to reflect LPV802 45
- Changed Figure 38 to reflect LPV802 45

Revision A History

Changes from Original (October 2015) to A Revision **Page**

- Changed from preview page 1

IMPORTANT NOTICE FOR TI REFERENCE DESIGNS

Texas Instruments Incorporated ('TI") reference designs are solely intended to assist designers ("Designer(s)") who are developing systems that incorporate TI products. TI has not conducted any testing other than that specifically described in the published documentation for a particular reference design.

TI's provision of reference designs and any other technical, applications or design advice, quality characterization, reliability data or other information or services does not expand or otherwise alter TI's applicable published warranties or warranty disclaimers for TI products, and no additional obligations or liabilities arise from TI providing such reference designs or other items.

TI reserves the right to make corrections, enhancements, improvements and other changes to its reference designs and other items.

Designer understands and agrees that Designer remains responsible for using its independent analysis, evaluation and judgment in designing Designer's systems and products, and has full and exclusive responsibility to assure the safety of its products and compliance of its products (and of all TI products used in or for such Designer's products) with all applicable regulations, laws and other applicable requirements. Designer represents that, with respect to its applications, it has all the necessary expertise to create and implement safeguards that (1) anticipate dangerous consequences of failures, (2) monitor failures and their consequences, and (3) lessen the likelihood of failures that might cause harm and take appropriate actions. Designer agrees that prior to using or distributing any systems that include TI products, Designer will thoroughly test such systems and the functionality of such TI products as used in such systems. Designer may not use any TI products in life-critical medical equipment unless authorized officers of the parties have executed a special contract specifically governing such use. Life-critical medical equipment is medical equipment where failure of such equipment would cause serious bodily injury or death (e.g., life support, pacemakers, defibrillators, heart pumps, neurostimulators, and implantables). Such equipment includes, without limitation, all medical devices identified by the U.S. Food and Drug Administration as Class III devices and equivalent classifications outside the U.S.

Designers are authorized to use, copy and modify any individual TI reference design only in connection with the development of end products that include the TI product(s) identified in that reference design. HOWEVER, NO OTHER LICENSE, EXPRESS OR IMPLIED, BY ESTOPPEL OR OTHERWISE TO ANY OTHER TI INTELLECTUAL PROPERTY RIGHT, AND NO LICENSE TO ANY TECHNOLOGY OR INTELLECTUAL PROPERTY RIGHT OF TI OR ANY THIRD PARTY IS GRANTED HEREIN, including but not limited to any patent right, copyright, mask work right, or other intellectual property right relating to any combination, machine, or process in which TI products or services are used. Information published by TI regarding third-party products or services does not constitute a license to use such products or services, or a warranty or endorsement thereof. Use of the reference design or other items described above may require a license from a third party under the patents or other intellectual property of the third party, or a license from TI under the patents or other intellectual property of TI.

TI REFERENCE DESIGNS AND OTHER ITEMS DESCRIBED ABOVE ARE PROVIDED "AS IS" AND WITH ALL FAULTS. TI DISCLAIMS ALL OTHER WARRANTIES OR REPRESENTATIONS, EXPRESS OR IMPLIED, REGARDING THE REFERENCE DESIGNS OR USE OF THE REFERENCE DESIGNS, INCLUDING BUT NOT LIMITED TO ACCURACY OR COMPLETENESS, TITLE, ANY EPIDEMIC FAILURE WARRANTY AND ANY IMPLIED WARRANTIES OF MERCHANTABILITY, FITNESS FOR A PARTICULAR PURPOSE, AND NON-INFRINGEMENT OF ANY THIRD PARTY INTELLECTUAL PROPERTY RIGHTS.

TI SHALL NOT BE LIABLE FOR AND SHALL NOT DEFEND OR INDEMNIFY DESIGNERS AGAINST ANY CLAIM, INCLUDING BUT NOT LIMITED TO ANY INFRINGEMENT CLAIM THAT RELATES TO OR IS BASED ON ANY COMBINATION OF PRODUCTS AS DESCRIBED IN A TI REFERENCE DESIGN OR OTHERWISE. IN NO EVENT SHALL TI BE LIABLE FOR ANY ACTUAL, DIRECT, SPECIAL, COLLATERAL, INDIRECT, PUNITIVE, INCIDENTAL, CONSEQUENTIAL OR EXEMPLARY DAMAGES IN CONNECTION WITH OR ARISING OUT OF THE REFERENCE DESIGNS OR USE OF THE REFERENCE DESIGNS, AND REGARDLESS OF WHETHER TI HAS BEEN ADVISED OF THE POSSIBILITY OF SUCH DAMAGES.

TI's standard terms of sale for semiconductor products (http://www.ti.com/sc/docs/stdterms.htm) apply to the sale of packaged integrated circuit products. Additional terms may apply to the use or sale of other types of TI products and services.

Designer will fully indemnify TI and its representatives against any damages, costs, losses, and/or liabilities arising out of Designer's non-compliance with the terms and provisions of this Notice.

Mailing Address: Texas Instruments, Post Office Box 655303, Dallas, Texas 75265